Progress in Nuclear Magnetic Resonance Spectroscopy xxx (xxxx) xxx

Contents lists available at ScienceDirect

Progress in Nuclear Magnetic Resonance Spectroscopy

journal homepage: www.elsevier.com/locate/pnmrs

The Dissolution-Dynamic Nuclear Polarization Experiment

Benno Meier *

Institute for Biological Interfaces 4, Karlsruhe Institute of Technology, 76344 Eggenstein-Leopoldshafen, Germany
Institute of Physical Chemistry, Karlsruhe Institute of Technology, 76131 Karlsruhe, Germany

ARTICLE INFO

Edited by Bradley Chmelka and Gareth Morris

Keywords:
Hyperpolarization
Dynamic Nuclear Polarization (DNP)
Dissolution-DNP
Temperature-jump DNP
Rapid-melt DNP
Bullet-DNP

ABSTRACT

Dissolution-Dynamic Nuclear Polarization (D-DNP) addresses the most pressing issue of nuclear magnetic resonance spectroscopy — low sensitivity. In D-DNP the analyte is mixed with a radical in a glass-forming matrix. This substrate is frozen and kept at low temperature (<100 K) and a magnetic field of several Tesla. By using microwave irradiation, polarization is transferred from electron spins to nuclear spins. The substrate is then liquefied, and the liquid-state signal of the nuclear spins is observed in a high-resolution nuclear magnetic resonance (NMR) magnet or a magnetic resonance imaging scanner. The D-DNP technique has enabled spectacular experiments, such as the *in vivo* observation of human metabolism. However, unlike other sensitivity enhancement methodologies, such as cryoprobes or magic angle spinning (MAS) DNP, D-DNP is not applied broadly in NMR spectroscopy at present. Here, we describe (i) the gains of an ideal D-DNP experiment for NMR spectroscopy, and contrast them with the real implementations of the D-DNP experiment available today, with a focus on applications in spectroscopy. We review principles of (ii) the dynamic nuclear polarization step and (iii) the sample transfer. We argue (iv) that stringent automation is essential for broader adaptation of the D-DNP experiment.

Contents

1. Introduction 2
2. The ideal vs. the real D-DNP experiment 3
3. Dynamic nuclear polarization 4
   3.1. Radicals 4
      3.1.1. Trityls 5
      3.1.2. BDPA 5
      3.1.3. Nitroxides 6
      3.1.4. UV- and other non-persistent radicals 6
      3.1.5. Oxygen 6
   3.2. DNP mechanisms 6
      3.2.1. The Overhauser effect 7
      3.2.2. The solid effect 7
      3.2.3. Triple spin flips 8
   3.3. The thermal mixing vs resonant mixing controversy 9
   3.4. Spin diffusion 9
   3.5. Heteronuclear polarization transfer for D-DNP 10
4. Sample transfer 11
   4.1. Original D-DNP 11
   4.2. Temperature-jump and rapid-melt DNP 11
   4.3. Bullet-DNP 12
5. Automation and the future 14
   Declaration of competing interest 14

* Correspondence to: Institute for Biological Interfaces 4, Karlsruhe Institute of Technology, 76344 Eggenstein-Leopoldshafen, Germany.
E-mail address: benno.meier@kit.edu.

https://doi.org/10.1016/j.pnmrs.2026.101598
Received 29 September 2025; Accepted 8 February 2026
Available online 9 February 2026

Acknowledgments 14
Data availability 14
References 14

1. Introduction

Nuclear magnetic resonance spectroscopy is a powerful and versatile technique, but its sensitivity is low because the NMR signal is often weak compared to the thermal noise in the NMR detector. The NMR signal is proportional to the polarization P of the nuclear spin states. For a spin 1/2 particle with a lower-energy state $+\frac{1}{2}$ and a higher-energy state $-\frac{1}{2}$, the polarization is given as

$$P = \frac{N_+ - N_-}{N_+ + N_-} \tag{1}$$

where N_+ and N_- denote the populations of the lower- and higher-energy state, respectively. The limiting values of P are thus -1 and $+1$ and correspond to spin systems in which all of the spins are in the $-\frac{1}{2}$ and $+\frac{1}{2}$-states, respectively.

At thermal equilibrium, the ratio of the populations of the two spin states is given by the Boltzmann distribution:

$$\frac{N_-}{N_+} = \exp\left(-\frac{\hbar\gamma B}{kT}\right). \tag{2}$$

Herein $\hbar\gamma B$ is the Zeeman energy, and kT is the thermal energy. The thermal equilibrium polarization P_{te} is then

$$P_{te} = \tanh\left(\frac{\hbar\gamma B}{2kT}\right) \tag{3}$$

For protons at 10 T and ambient temperature, the thermal equilibrium polarization is $P_{te} \approx 3.4\times10^{-5}$, i.e. it is four orders of magnitude smaller than its theoretical maximum value of +1.

Hyperpolarization techniques seek to move the polarization closer to unity, and thereby enhance the NMR signal strength. A comprehensive review of the full variety of hyperpolarization techniques has recently been given by Eills, Koptyug and co-workers [1]. For a detailed discussion of NMR sensitivity with and without hyperpolarization, we refer to our recent article [2].

The simplest way to increase the polarization is to lower the temperature. This is not *per se* a hyperpolarization technique, since one still operates at thermal equilibrium. If, however, one requires a measurement under ambient conditions, one may polarize the nuclei at a very low temperature, and then increase the temperature rapidly. This approach is known as "brute-force" hyperpolarization [3,4]. One may see from Eq. (3) that, at a field of 10 T, a temperature of 100 mK is required to achieve a thermal equilibrium polarization of 10% for protons. A key challenge of brute-force hyperpolarization is that the spin-lattice relaxation time constant becomes very long at low temperatures. Hirsch and co-workers observed that approximately 65% of P_{te} can be achieved by equilibrating 1-^{13}C-labeled pyruvic acid at 14 T and 2.7 K for 24 h, but less than 5% of P_{te} can be attained when the same procedure is carried out at a temperature of 0.5 K [3].

The source of polarization in dynamic nuclear polarization is the thermal equilibrium polarization of the electron spin. Free electron spins are usually added to the sample in the form of a stable free radical, referred to as polarizing agent (PA). The PAs that are typically used in DNP have a g-factor close to 2, and therefore a gyromagnetic ratio that is 660 times larger than that of the proton. Consequently, unpaired electrons exhibit near unity spin polarization in a field of several Tesla at temperatures of the order of 1 K. The relevant interactions in DNP are the Zeeman interactions of both the electron and the nuclear spins, the hyperfine coupling between electrons and nuclei, nuclear–nuclear dipolar couplings and, in certain cases, electron–electron couplings. The large electron Zeeman interaction generates a large thermal equilibrium electron spin polarization. This polarization can be transferred to a nearby nucleus via a "DNP mechanism", which always requires the simultaneous presence of an electron–nuclear hyperfine interaction and microwave irradiation. Some DNP mechanisms, however require the presence of a second electron spin, with a coupling to the first electron spin, or the presence of a specific cross-relaxation mechanism. Subsequently, nuclear dipole–dipole couplings drive spin diffusion, leading to a polarization of the entire sample.

The DNP mechanisms that are used in D-DNP are discussed in detail in Part 2. Briefly, we distinguish the "Overhauser effect" (OE), the "solid effect" (SE) and "triple spin flip (TSF) DNP". In the Overhauser effect, one saturates an electron transition, thereby equilibrating the populations of the lower- and higher-energy electron spin state. Subsequently, cross-relaxation is required to produce an enhanced nuclear spin polarization. In insulating solids, cross-relaxation is absent, but it is possible to drive forbidden electron–nuclear flip-flops (as first shown independently by Jeffries [5] and Abragam and co-workers [6]) via the solid effect. In triple spin flip DNP, the microwave inverts a single electron spin, followed by an electron–electron–nuclear triple spin flip that drives the nuclear spin polarization. As described in greater detail in Part 2, the cross-effect and thermal mixing are both limiting cases of triple spin flip DNP. A number of laboratories are exploring time-domain DNP, which would establish a coherent polarization transfer similar to the INEPT (Insensitive Nuclei Enhanced by Polarization Transfer) or cross-polarization (CP) sequences which are well known in liquid- and solid-state NMR [7–10]. DNP may also be combined with light irradiation: In triplet-DNP, one uses light to first pump the electron spin polarization, which is only then transferred to the nuclei using DNP [11,12]. In all DNP techniques, nuclear spin polarization is generated in the vicinity of a free electron spin, and spin diffusion is required to distribute the nuclear spin polarization across the sample. We discuss spin diffusion in Part 2, but note that the diffusion process itself can give access to structural information [13,14].

As the name implies, DNP is the hyperpolarization method of choice in the D-DNP experiment. However, other hyperpolarization techniques that produce a hyperpolarized solid can in principle be combined with a dissolution step to yield an experiment that, like D-DNP, enhances the liquid-state NMR signal.

The high nuclear-spin polarization that can be achieved optically in naphthalene has already been used to sensitize liquid-state NMR [12,15]. In the solid-state photo-CIDNP effect, a radical pair is created transiently by irradiating a suitable precursor with light [16]. The subsequent evolution and recombination of the radical pair drives the polarization of a nearby coupled nuclear spin and, via spin diffusion, the polarization of an entire spin bath. Recently, it was shown that tailored molecules drive this process efficiently at high field [17,18]. Combining photo-CIDNP with dissolution for liquid-state NMR signal enhancement is an attractive proposition, given the ease and low cost with which light irradiation can be implemented.

In parahydrogen-induced polarization (PHIP), a pure spin state is achieved using the large rotational splitting of the hydrogen molecule [19,20]. Here, one uses the Pauli principle that requires the overall wavefunction of the two proton fermions to be antisymmetric. As a consequence, a pure rotational state with all hydrogen molecules in the rotational ground state is associated with a pure singlet state of the molecule's nuclear spins. While singlet hydrogen is NMR-invisible, a reaction – followed by evolution under the spin Hamiltonian – may be used to convert the singlet order into highly polarized spin states. As shown by Duckett and co-workers [21], this process can also be carried out in a reversible way. Molecules polarized with PHIP may be condensed and solidified with other target molecules to enable polarization transfer in the solid via spin diffusion, and upon subsequent

dissolution, the target molecules retain hyperpolarization [22]. The niche field of quantum-rotor-induced polarization (QRIP) like PHIP uses the large rotational splitting of a rotor that is able to rotate freely at temperatures small compared to the rotational splitting. Examples are freely rotating methyl groups or freely rotating molecules such as fullerene-encapsulated water, $H_2O@C_{60}$. In QRIP, cross-relaxation processes replace the chemical reaction as the key to generating polarized nuclear spin states [23,23–28]. The same processes that give rise to QRIP are active in many DNP samples with methyl groups, and they may be critical for a quantitative understanding of relaxation in particular during the transfer of hyperpolarized solids. The relaxation properties of methyl groups can also be put to use for structural elucidation in MAS DNP [29,30].

In the dissolution-dynamic nuclear polarization (D-DNP) experiment, the large thermal equilibrium spin polarization of the electron spins is transferred to nuclear spins using microwave irradiation at a temperature of typically 1–2 K. Subsequently the sample is dissolved or liquefied, yielding a solution in which the nuclear spins retain a high, non-equilibrium spin polarization.

Dissolution-DNP was invented by Ardenkjær-Larsen, Golman and co-workers [31]. Indeed the first *in vivo* MRI observation of human metabolism in prostate cancer was reported in 2013 [32], only 10 years after its inventors had published their initial report. In their study, Nelson and co-workers were able to track the conversion of hyperpolarized pyruvate to lactate in the living human body. Any treatment of cancerous tissue would affect tumor metabolism, and thus hyperpolarized MRI may become a powerful diagnostic tool to assess the response to cancer treatment in a timely manner [33–38].

Dissolution-DNP has found notable applications also in NMR *spectroscopy*, but, like other liquid-state hyperpolarization technologies, it has so far remained a relatively specialized technique. By comparison, methods that increase the sensitivity of liquid-state NMR *without* hyperpolarization, i.e. at thermal equilibrium, have found widespread use. For example cryoprobes offer a sensitivity enhancement of a factor of 4, which may seem modest compared to what dissolution-DNP seems to offer, yet their use is standard practice in high-field liquid-state NMR. In this article, however, we take the view that D-DNP may become a much more widely used research tool for NMR spectroscopy.

In Part 1 we compare what we call the *ideal* D-DNP experiment with the current state of the art, which we call the *real* D-DNP experiment. The ideal D-DNP experiment is an experiment that would provide all the advantages of D-DNP, and none of the disadvantages. Such an experiment may perhaps never be realized, but its description facilitates the subsequent identification of the most pressing challenges of the real D-DNP experiments available today. The remainder of this article discusses the current state of affairs with respect to these challenges. In Part 2 we review the DNP process itself, and associated strategies to achieve a high solid-state nuclear spin polarization in a short time. We review the dependence of polarization level on magnetic field, temperature, sample composition and radical, as well as on dynamic parameters such as microwave frequency sweeps and cross-polarization. In Part 3 we review different implementations of the D-DNP experiment. Note that we use the term "D-DNP experiment" both for the original implementation by Ardenkjær-Larsen et al. as well as for all implementations that use DNP for hyperpolarization, followed by a melting/dissolution step and liquid-state NMR acquisition. These are broadly classified as (i) the "original" D-DNP experiment developed by Ardenkjær-Larsen and co-workers (referred to as "original" D-DNP, when the delineation to other implementations is critical), (ii) temperature-jump DNP (TJ-DNP) and rapid-melt DNP (RM-DNP) developed by the groups of Griffin and Kentgens, respectively, and (iii) a solid transfer such as we reported with bullet-DNP (B-DNP). In Part 4 we briefly discuss the subject of automation.

We will discuss the advantages and disadvantages of each of the above-mentioned implementations of D-DNP for NMR spectroscopy. Applications of D-DNP are not covered in detail in this review article.

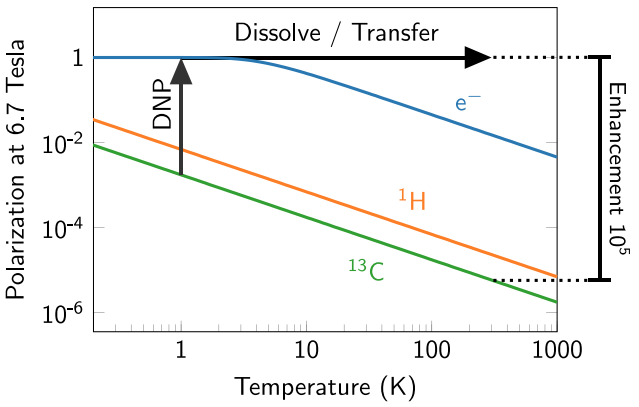

Fig. 1. The D-DNP Experiment. For a field of 6.7 T, the temperature-dependent thermal equilibrium polarizations of electrons, protons, and ^{13}C nuclei are shown in blue, orange, and green, respectively. The D-DNP experiment progresses in a clockwise manner: Firstly, the high electron spin polarization is transferred to nuclei via microwave irradiation. Secondly the sample is liquefied and transferred to a highly homogeneous magnetic field where an NMR spectrum is recorded, with signals that are up to five orders of magnitude larger than their thermal equilibrium counterparts.

For applications in NMR spectroscopy and metabolomics we refer the reader to recent articles by the group of Hilty [39,40] and by Jannin et al. [41]. For practical aspects of D-DNP experiments we refer to a recent review by the group of Jannin [42]. A review of D-DNP methodology with a focus on instrumentation and sample formulation has been given by Pinon et al. [43]. For applications of D-DNP in MRI, and in particular human *in vivo* applications the reader is referred to recent reviews by Kurhanewicz et al. [35] and Ardenkjær-Larsen [44].

2. The ideal vs. the real D-DNP experiment

The ideal D-DNP experiment

The concept of the D-DNP experiment is shown in Fig. 1. Electrons are fully polarized in a magnetic field of several Tesla at a temperature of approximately 1 K. In the dynamic nuclear polarization step the electron spin polarization is transferred to nuclei such as ^1H or ^{13}C using microwave irradiation. Subsequently the sample is liquefied and transferred, and a liquid-state NMR spectrum with a signal enhancement of several orders of magnitude is recorded.

The ideal D-DNP experiment has the following characteristics: (i) Substrates with fully polarized nuclei such as ^1H, or ^{13}C can be provided with a duty cycle or repetition time that is shorter than the acquisition time required for a single spectrum, such that a fully hyperpolarized sample is available for each acquisition. (ii) The transfer of the sample from the point of polarization to the point of detection of the spectrum occurs without loss of polarization. (iii) The liquefaction of the sample occurs without dilution. (iv) The liquefied sample is free of any unwanted species, such as radicals, glassing agents or gas bubbles, and yields spectra that are of equal quality compared to their counterparts recorded under static conditions. (v) Additionally, the ideal D-DNP experiment exhibits the characteristics (i) to (iv) irrespective of the substrate volume.

In the ideal D-DNP experiment, the sensitivity gain S corresponds directly to the signal enhancement ϵ, which is the ratio of the hyperpolarized spin polarization P_{hyp} and its thermal equilibrium counterpart P_{te}. Consider an experiment with hyperpolarized ^{13}C, detected in an 11.7 T field, corresponding to a ^1H Larmor frequency of 500 MHz. The thermal equilibrium polarization is then $P_{te}(^1H, 11.7\ T, 300\ K) \approx 4 \times 10^{-5}$ for ^1H and $P_{te}(^{13}C, 11.7\ T, 300\ K) \approx 1 \times 10^{-5}$ for ^{13}C.

The enhancement ϵ is defined as the ratio of the polarization of the hyperpolarized sample P_{hyp} and the polarization in thermal equilibrium P_{te}.

In favorable cases, D-DNP can achieve near unity spin polarization. Then, the sensitivity gain S_{ideal} is given by the enhancement ϵ, which, for detection of ^{13}C at 11.7 T and 300 K evaluates to

$$S_{\text{ideal}} = \epsilon = \frac{P_{\text{hyp}}}{P_{\text{te}}} = \frac{1}{P_{\text{te}}} \sim 10^5, \tag{4}$$

In the ideal D-DNP experiment the sensitivity gain is equal to the signal enhancement. It is well known that sensitivity may also be gained in thermal equilibrium (hereafter referred to as static NMR), by using signal averaging. In this case the signal increases linearly with the number of scans N, the noise increases as $\sqrt{N}$, and so the signal-to-noise ratio (SNR) increases as $\sqrt{N}$. Thus a prohibitive number of 100 million scans would be required to achieve the same sensitivity as the ideal D-DNP experiment. From this analysis it may seem that D-DNP would clearly outperform static NMR even if it offered a much lower sensitivity gain. Why then is D-DNP not in widespread use?

The real D-DNP experiment

Several differences between the ideal D-DNP experiment and its various realizations lead to a substantial reduction of the sensitivity gain. A typical realization today has the following characteristics: (i) Approximately one hyperpolarized sample can be provided every 2 h, owing to the required time for the DNP process to complete. Other rate-limiting factors are the cooling capacity of the instrument or the availability of personnel to run the experiment. (ii) For sample volumes in the range of 1–10 μL, a typically 100-fold dilution occurs prior to detection, owing to the need to provide sufficient heat to melt the frozen material in the cold space of the cryostat or the need to fill the NMR tube of a conventional NMR probe. While dilution also reduces the radical concentration and hence radical-induced relaxation, it directly reduces the mass-sensitivity of the measurement. (iii) The loss of spin polarization during the transfer is significant, in particular for high-γ nuclei and large molecules with short nuclear spin relaxation time constants. (iv) Radicals and glassing agents are present in the liquefied sample, and bubbles degrade the quality of the recorded spectra.

These characteristics reduce the sensitivity gain that is available in a real experiment. The latter may be estimated by assuming that under static conditions one spectrum is recorded every 10 s, leading to a 720-fold slower throughput if the DNP experiment is carried out every 2 h. This implies that in the same time the sensitivity of the static experiment can be increased by a factor of $\sqrt{720}$ via averaging 720 scans. We also assume that the signal enhancement ϵ is 10,000, and that the observed linewidth is broadened from 1 Hz to 10 Hz. Apart from obscuring spectral information such an increase in linewidth leads to a loss in sensitivity as the increased spectral range contains more noise by a factor (after adjusting apodization, see Ref. [2] for a detailed analysis) of $\sqrt{10}$. Thus, scaling the ideal sensitivity gain for dilution, signal averaging and increased linewidth, we get

$$S_{\text{real}} = \frac{\epsilon}{100\sqrt{720}\sqrt{10}} = \frac{10,000}{100\sqrt{720}\sqrt{10}} \sim 1 \tag{5}$$

Note that even at unity sensitivity gain, DNP can enable NMR investigations for processes that happen to fast for signal averaging, but that are on the same time scale or faster than the nuclear spin lattice relaxation time constant [45–47]. However, it follows from Eq. (5), that at present D-DNP is not (yet) a generally applicable sensitivity enhancement technique. In fact, despite a 10,000-fold larger polarization our typical D-DNP experiment has the same sensitivity that would be obtained with static acquisition and standard signal averaging. Below, the factors contributing to the sensitivity gain of the real D-DNP experiment are briefly discussed.

Enhancement. The enhancement ϵ is directly proportional to the achieved spin polarization. Substantial progress has been achieved with respect to the polarization step. Both the final polarization level and the rate at which the polarization builds up depend on magnetic field, temperature, sample composition, and the process of hyperpolarization (frequency-swept or static, and, for low-γ nuclei direct polarization, or indirect polarization via protons). The polarization level has received considerable attention, and continues to be an important metric for any realization of the D-DNP experiment. Typical enhancement values for ^{13}C are 5000 to 50,000. For protons, enhancements are substantially smaller, and typically below 1000.

Dilution. The sensitivity gain of a D-DNP experiment depends critically on whether the dilution enters the sensitivity analysis or not. In fact, important applications of D-DNP arise in particular when an analyte can be polarized at high concentration, but needs to be studied at low concentration. This is often the case for *in vivo* studies where analytes like pyruvate or glucose are polarized at high concentrations, but where the acceptable concentration in the living organism is limited and achievable despite the dilution of the substrate that occurs in the D-DNP process. Studies of ligand-binding likewise require a low concentration of hyperpolarized ligands [48]. Generally, if an equal or greater dilution would be required also for the static experiment, the factor d in Eq. (5) has to be set to unity, since the D-DNP experiment can be carried out at the same final concentration as the static experiment. In this case the transformative gain in sensitivity is immediately obvious. D-DNP may also compare favorably to static NMR when transient processes, for instance in reaction monitoring, are observed. For a more detailed discussion of the dilution factor the reader is again referred to Ref. [2].

Throughput. With the notable exception of temperature-jump and rapid-melt DNP (see Section 4.2), the throughput of D-DNP today is low. Again this limitation is not of great significance for *in vivo* measurements where significant time is required for the preparation of animals or human patients. The throughput of D-DNP in spectroscopy is typically limited by long polarization times, as well as the time to prepare the experiment (and clean the system after each use) [49]. As the throughput of D-DNP is increased substantially (for example through parallelized polarization), the heat load during sample loading and ejection has to be taken into account as well.

Resolution. NMR spectra gain not only resolution but also sensitivity from the use of highly homogeneous fields that enable precession of the magnetization over seconds without dephasing, giving rise to sub-Hz resolution. In D-DNP experiments, the requirement to rapidly melt and/or transfer the sample often introduces bubbles or other inhomogeneities, and, when using aqueous solvents, linewidths are a little or much above 1 Hz, depending on how much effort is spent on achieving high resolution.

Regarding the sensitivity gain, it is instructive to compare D-DNP with MAS-DNP. In MAS-DNP, typical enhancements are of the order of 100, with a maximum ^{1}H enhancement of 660. However, there is no substantial dilution, the loss in spectral quality is limited, and the throughput can even be enhanced because the polarization buildup rate is faster than the longitudinal spin-lattice relaxation rate. As a consequence, MAS-DNP is in widespread use as a general sensitivity enhancement technique for solid-state NMR.

3. Dynamic nuclear polarization

3.1. Radicals

In dynamic nuclear polarization, nuclear spin hyperpolarization is achieved by transferring polarization from electron to nuclear spins. The electron spin is usually supplied in the form of a stable radical, which is also referred to as a polarizing agent (PA).

Typical polarizing agents used in D-DNP are shown in Fig. 2, their g- and hyperfine tensors are given in Table 1. Radical data for TEMPO are taken from [50], for TEMPOL from [51], for trityl from [52], for BDPA from [53], for pyruvic acid irradiated with ultraviolet light (UV-PA) from [54]. Note that for axially symmetric tensors like trityl, the

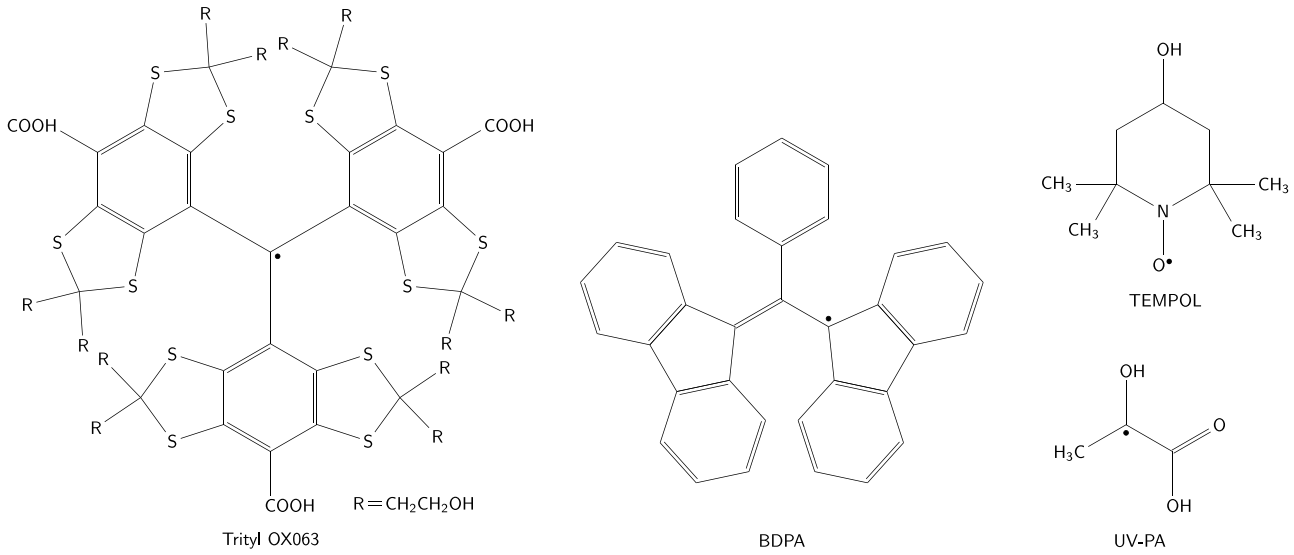

Fig. 2. Radicals commonly used in D-DNP. The narrow-band radicals OX063 (left) and BDPA (center) are used for directly polarizing low-γ nuclei such as ^{13}C, while nitroxide radicals like TEMPOL (top right) are used for polarizing high-γ nuclei (^{1}H and ^{19}F). A ketyl radical of pyruvic acid (bottom right) may be generated via irradiation with ultra-violet light. In this case, the EPR spectrum can be tuned considerably via hyperfine interactions that can be introduced by ^{13}C labeling [54].

notation $g_\perp = g_x = g_y$, $g_\parallel = g_z$ is often used. The nitroxide hyperfine interaction is due to the ^{14}N spin. The small hyperfine interactions of trityl to its remote protons have been ignored.

The radicals that are used in D-DNP experiments can be classified broadly into broad-band and narrow-band radicals. Broad-band radicals like TEMPOL exhibit an EPR spectrum that is of the same width or wider than the ^{1}H Larmor frequency. Narrow-band radicals exhibit an EPR spectrum that is narrow compared to the ^{1}H Larmor frequency. When the width of the EPR spectrum matches the nuclear Larmor frequency, the radical optimally supports triple spin flips. Triple spin flips are explained below, and are the prevailing DNP mechanism in D-DNP. Therefore, the broad-band nitroxide radicals are used widely for polarizing protons, and the narrow-band radicals are used widely for polarizing ^{13}C spins.

Fig. 3 shows simulated EPR spectra of the nitroxide radical TEMPOL and the trityl radical OX063 as representatives of these two classes of radicals at various fields. At high frequencies, the spectrum is broadened by g-anisotropy, with the hyperfine coupling causing the characteristic shoulders to the left of the spectrum. At all fields, the TEMPOL spectrum is broad compared to the ^{13}C and ^{1}H Larmor frequencies (indicated by the green and orange lines, respectively). TEMPOL spectra were simulated using Gaussian kernels with $\sigma = 10$ MHz. The narrow-band trityl spectra are likewise broadened by g-anisotropy, but the anisotropy is substantially smaller, and, at 94 GHz and higher, the width of the spectrum is comparable to the ^{13}C Larmor frequency. The simulations do not include any broadening due to electron–electron interactions (which would depend on the concentration of the radical, see [55]) or due to hyperfine interactions to nitroxide protons or nuclear spins in the solvent. At 9 GHz the spectrum is broadened by the ^{14}N hyperfine coupling. OX063 spectra were simulated using Gaussian kernels with $\sigma = 2$ MHz. Note that *cw*-EPR spectra are often measured at fixed frequency by sweeping the field. To transform the spectra shown here to field-swept EPR spectra, one has to take the derivative of the spectrum and reverse the x-axis. All spectra were simulated using Spinthon [56].

The importance of the choice of radical for achieving a high polarization cannot be overstated. As will be discussed in the following section, different radicals support different DNP mechanisms, but the DNP mechanisms at play will also depend strongly on the strength of the applied magnetic field as well as the power of the available microwave source. The electron spin T_1 needs to be sufficiently fast to drive repeated electron–nuclear polarization transfer, and sufficiently long such that an electron spin transition can be saturated with the available microwave power. Hess and co-workers found that at a temperature of 1 K and a field of 2.5 T, the electron spin-lattice relaxation rate in butanol scales linearly with the radical concentration, according to $1/T_1 \sim 200$ [R]/s, where [R] is the molar radical concentration [57]. Remarkably, the same scaling applied for both TEMPO and trityl and was observed for both protonated and deuterated butanol. Thus, for a 50 mM concentration, an electron $T_1 \sim 0.1$ s results. Following the polarization step, the electron spin of the radical is no longer needed, but it may now cause unwanted, fast nuclear spin relaxation. An intriguing variety of strategies has been developed to reduce such relaxation to the largest extent possible. We briefly discuss various radicals before elaborating on the DNP mechanisms that they support.

3.1.1. *Trityls*

The trityl radical OX063 was used in the original work by Ardenkjær-Larsen, Golman and co-workers to directly polarize ^{13}C at a field of 3.35 T [31]. Under these conditions, the dominant DNP mechanism is the solid effect. As the field is increased to 6.7 T, the DNP spectrum indicates that triple spin flips drive the DNP process [58]. The narrow-band trityl radical is typically used at concentrations of 15 mM for polarizing low-γ nuclei like ^{13}C. However, when the concentration approaches 100 mM, inter-radical interactions substantially broaden the EPR line, and proton polarization via triple spin flips becomes possible [55,59]. It is also possible to polarize protons using low trityl concentrations via the solid effect. However, it appears that only klystrons and gyrotrons are currently able to provide enough microwave power to do so in the non-resonant setups that are used in D-DNP experiments [60]. Trityl causes moderate nuclear spin relaxation in solution at high magnetic fields [61].

3.1.2. *BDPA*

BDPA [53,62] is, like trityl, a narrow-line radical, but its DNP spectrum indicates an Overhauser effect [63], which persists even at temperatures as low as 1.2 K [64]. It may be sulfonated to make it water soluble. Unmodified BDPA may be dissolved in polystyrene or ortho-terphenyl [64]. It was also dissolved in glass-forming mixtures of sulfolane and polyethylene glycol together with small molecules of interest [65]. An attractive feature of this formulation is that the radical precipitates upon dissolution with water, preventing radical-induced relaxation after the dissolution.

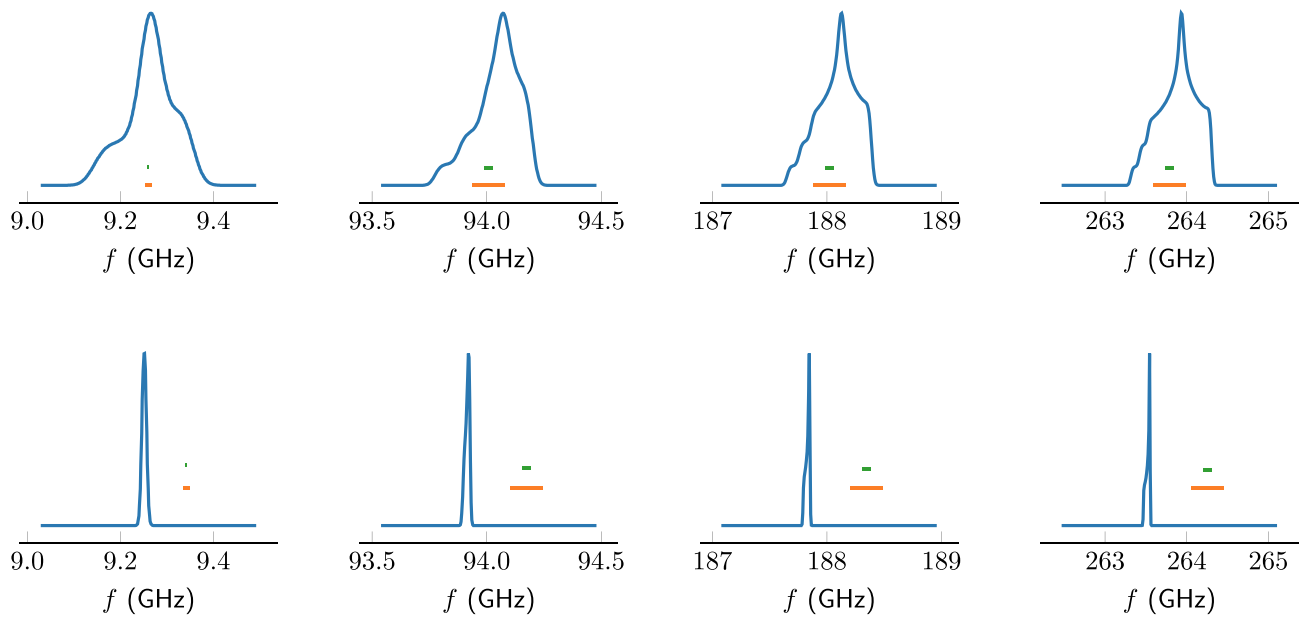

Fig. 3. Simulated EPR Spectra for the broadband radical TEMPOL (top) and the narrow-band trityl radical 0X063 (bottom) at 0.33 *T* (X-band, far left) and fields that are commonly used in D-DNP experiments (3.35 T, 6.7 *T* and 9.4 T, from left to right). At 0.33 *T* (9 GHz), the TEMPOL spectrum is strongly broadened by the ^{14}N hyperfine coupling.

Table 1
g anisotropies and hyperfine tensors (in MHz) for radicals frequently used in D-DNP. *Note that the spectrum of perdeuterated BDPA can be modeled more accurately assuming two hyperfine tensors with principal components of the order of 1 MHz or less due to couplings of the delocalized electron spin to two sets of equivalent protons on the two fluorene moieties, the procedure is described in Ref. [53]. **The hyperfine tensor of UV-PA can be tuned considerably using ^{13}C labeling [54].

Radical	g_x	g_y	g_z	A_{xx}	A_{yy}	A_{zz}
TEMPO	2.0094	2.0065	2.0017	20.5	17.7	101
TEMPOL	2.008	2.005	2.001	24.23	16.96	103.33
Trityl (OX063)	2.00319	2.00319	2.00258	–	–	–
BDPA	2.00263	2.00259	2.00234	-*	-*	-*
UV-PA	2.0036	2.0027	2.0007	-**	- **	- **

3.1.3. Nitroxides

Nitroxides like TEMPO and TEMPOL are used widely for polarizing high-γ nuclei like protons, typically at concentrations of 50 mM. While nitroxides may be used to polarize low-γ nuclei directly to fairly high levels [66], they are frequently used to first polarize protons and then transfer the proton polarization to the lower-γ nuclei (see Section 3.5). Nitroxides can cause fast nuclear spin relaxation in solution, but can be scavenged with ascorbic acid [67,68]. Nitroxides may be immobilized on silica to prevent them from causing nuclear spin relaxation in the liquid phase [69,70]. It is also possible to control the distance between the radicals and nuclei by using hydrogels [71,72] or epoxy resins [73].

3.1.4. UV- and other non-persistent radicals

An intriguing approach to preventing radical-induced relaxation of hyperpolarized nuclear spins after dissolution is to use non-persistent radicals. Keto-group bearing molecules like pyruvate [74], α-keto-glutarate and others [75] may be transformed into radicals by exposing them to high-intensity ultra-violet light at low temperatures. The radicals are stable at liquid nitrogen temperature but are quenched when they are heated to ambient temperature. The width of the EPR line of the radicals can be tuned by adjusting the hyperfine coupling between the electron spin and neighboring nuclei by using spin labels [54,76]. This concept has also been extended to visible light, which is less prone to damage the substrate [77].

Other non-persistent radicals include Frémy's salt [78], radicals generated by electric discharge [79], and radicals generated by γ-irradiation [80,81].

3.1.5. Oxygen

Another radical that is often present in DNP samples is molecular oxygen [82]. As shown in Fig. 4, the low-temperature electron T_1 of trityl is governed by the concentration of oxygen in the sample [57], and also the proton T_1 (in the absence of broadband radicals) at medium and high-field is often determined by oxygen [4]. Molecular oxygen exhibits a zero field splitting of the order of 100 GHz and can thus couple to phonons even at low magnetic field, enabling relaxation. The large zero-field-splitting of molecular oxygen represents an opportunity for efficient dynamic nuclear polarization at near zero field. Experiments to test this approach are currently being prepared in our lab.

3.2. DNP mechanisms

The radicals discussed in the previous section are the source of polarization in DNP. The transfer of polarization from a radical to a nucleus always occurs by transitions between electron spin states and can take place in one of three different ways. In the Overhauser effect, microwave irradiation is applied on resonance, and drives a single electron-spin flip, followed by electron–nuclear cross-relaxation. In the solid-effect, the microwave irradiation is applied off-resonance, and drives an electron–nuclear flip-flop, thereby directly hyperpolarizing the nuclear spins. Most D-DNP experiments rely on the third family of DNP mechanisms, which is the family of triple spin flips. In triple spin flips, an electron–electron flip-flop is accompanied by a nuclear flip. The role of the microwave is to invert some of the electron spins, so that

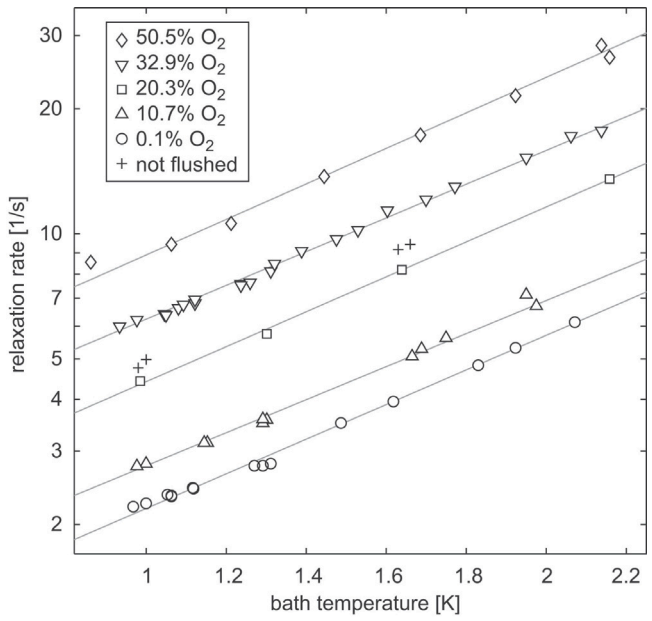

Fig. 4. The electron spin-lattice relaxation rate of trityl-doped D-butanol samples at low temperatures and 2.5 T is determined by the oxygen content. Figure reproduced from Ref. [57] with permission.

the electron–electron flip-flops actually become possible. As detailed in Section 3.2.3, the cross effect (CE) and thermal mixing (TM) are special cases of triple spin flips.

A general comment is now due regarding the construction of Hamiltonians in dynamic nuclear polarization. The usual procedure is to first consider the Hamiltonian $\mathcal{H}_0$ of the spin system in the absence of microwave irradiation. This Hamiltonian is then diagonalized and the energy structure of the spin system is obtained. In a second step one considers the effect of applying microwave irradiation via an additional Hamiltonian $\mathcal{H}_1$. The Hamiltonian $\mathcal{H}_1$ is not diagonal in the eigenbasis of $\mathcal{H}_0$, and hence drives transitions between the eigenstates of $\mathcal{H}_0$. Electron–nuclear transitions are always mediated by the truncated hyperfine coupling. A rigorous truncation procedure for spin–spin interactions that considers the combined action of static and oscillating magnetic fields has been given by Fine [83,84].

A standard way to explore DNP mechanisms in experiment is to measure the so-called DNP spectrum D. Here, one saturates the nuclear spin polarization, and then records its intensity after a fixed time of microwave irradiation. By varying the frequency of the microwave irradiation ω, the DNP spectrum $D(\omega)$ is obtained. We note that $D(\omega)$ depends weakly on the buildup time [58].

3.2.1. The Overhauser effect

The Overhauser effect, shown in Fig. 5, was predicted by Overhauser [85] and demonstrated by Carver and Slichter [86,87]. Assuming that the hyperfine interaction is small compared to both the electron and the nuclear Zeeman interaction, the eigenstates of the Overhauser spin system are approximately the product states of the electron and the nuclear Zeeman interaction, i.e., the Hamiltonian may be written as [88]

$$\mathcal{H}_0 = -\omega_{0I}\hat{I}_z + \omega_{0S}\hat{S}_{1z} + A\hat{I}_z\hat{S}_{1z}. \tag{6}$$

Here, $\hat{I}_z$ and $\hat{S}_{1z}$ are the spin operators of the nuclear and the electron spin, respectively, ω_{0I} and ω_{0S} are their Larmor frequencies, and A is the truncated hyperfine coupling. In the Overhauser effect, a microwave field is used to saturate a pure electron spin transition. The existence of a cross-relaxation process, in which an electron spin flip and a nuclear spin flip occur simultaneously, then leads to enhanced polarization across nuclear spin levels. The Overhauser effect was first shown in lithium metal, where the Fermi contact interaction drives electron–nuclear flip-flops. In liquids, it is the modulation of dipolar coupling terms such as I^+S^- and I^+S^+, brought about by the molecular motion, that provides the required cross-relaxation process [89]. If the target molecule can bind reversibly to a radical, the scalar part of the electron–nuclear interaction is also modulated, thereby providing an alternative pathway for achieving nuclear spin hyperpolarization. The scalar interaction only drives flip-flop transitions, and is itself field-independent [90]. However, the polarization enhancement due to the scalar interaction becomes suppressed at high field in the presence of the competing dipolar mechanism [91]. The characteristic feature of the Overhauser effect, an increase in nuclear spin polarization upon on-resonant excitation of the electron spin, has also been observed in insulating solids doped with BDPA, and has been linked to the strong hyperfine couplings present in BDPA [63,92]. The Overhauser effect has also been observed under D-DNP conditions, and various mechanisms have been suggested to drive the required modulation of the hyperfine couplings [64].

Since the Overhauser effect relies on saturation of the EPR resonance, its DNP spectrum $D^{\mathrm{OE}}(\omega)$ scales directly with the EPR spectrum $S(\omega)$:

$$D^{\mathrm{OE}}(\omega) \sim S(\omega) \tag{7}$$

3.2.2. The solid effect

Rather than relying on a strong electron–nuclear cross-relaxation effect, in the solid effect, one hyperpolarizes nuclear spins directly by driving so-called forbidden transitions. This mechanism is shown in Fig. 6. It was first described by Jeffries [5], and developed and demonstrated independently by Abragam, Combrisson and Solomon [6] who called it the "effet solide". Erb et al. discovered the effect independently as well [93]. The solid effect spin system comprises the electron and the nuclear Zeeman interaction, and a hyperfine interaction:

$$\mathcal{H} = -\omega_{0I}\hat{I}_z + \omega_{0S_1}\hat{S}_{1z} + \hat{\boldsymbol{S}}_1\boldsymbol{A}\hat{\boldsymbol{I}} \tag{8}$$

Here, $\hat{\boldsymbol{I}} = (\hat{I}_x, \hat{I}_y, \hat{I}_z)$ and $\hat{\boldsymbol{S}}_1 = (\hat{S}_{1x}, \hat{S}_{1y}, \hat{S}_{1z})$ are the vector spin operators of the nuclear and the electron spin, respectively, ω_{0I} and ω_{0S} are their Larmor frequencies, and $\boldsymbol{A}$ is the hyperfine tensor. The energy diagram in Fig. 6 assumes that the hyperfine interaction is small compared to the electron and nuclear Zeeman interactions. But since $\boldsymbol{A}$ is non-zero, the product states of the nuclear and electron Zeeman states are not the exact eigenstates of the Hamiltonian. As a consequence, the electron–nuclear transitions are not strictly forbidden. As the applied magnetic field is increased, the product states increasingly correspond to the true eigenstates of the Hamiltonian, and the solid effect gets weaker and weaker. Using solid-state microwave sources with an output power of the order of 100 mW as typically used in D-DNP, a solid effect is observed when polarizing low-γ nuclei at 3.35 T, but at 6.7 T no significant polarization is attained via this mechanism. Using more powerful microwave sources, it is however possible to observe a solid effect at higher fields [60].

Assuming a small hyperfine interaction and ignoring spin diffusion, the DNP spectrum of the solid effect scales as

$$D^{\mathrm{SE}}(\omega) \sim S(\omega - \omega_I) - S(\omega + \omega_I) \tag{9}$$

If the EPR line is narrow compared to the nuclear Larmor frequency, the DNP spectrum displays a well-resolved solid-effect, with positive enhancement at a microwave frequency $\omega = \omega_{0S_1} - \omega_{0I}$, and a negative enhancement at a frequency of $\omega = \omega_{0S_1} + \omega_{0I}$. As the EPR line gets wider, the lines in the DNP spectrum start to widen. When the EPR linewidth is larger than the nuclear Larmor frequency, the DNP enhancement becomes a continuous function of the microwave frequency. If electron spin-diffusion can be neglected, it is then possible that both positive and negative DNP processes are driven simultaneously, leading to a reduction in the overall enhancement. It is also possible to drive transitions in which one electron spin and *two* nuclei flip simultaneously. This effect is known as the three-spin solid effect [94].

The first D-DNP experiments were conducted using DNP at 3.35 T, and trityl radicals for hyperpolarizing ^{13}C. For this system, a clear solid

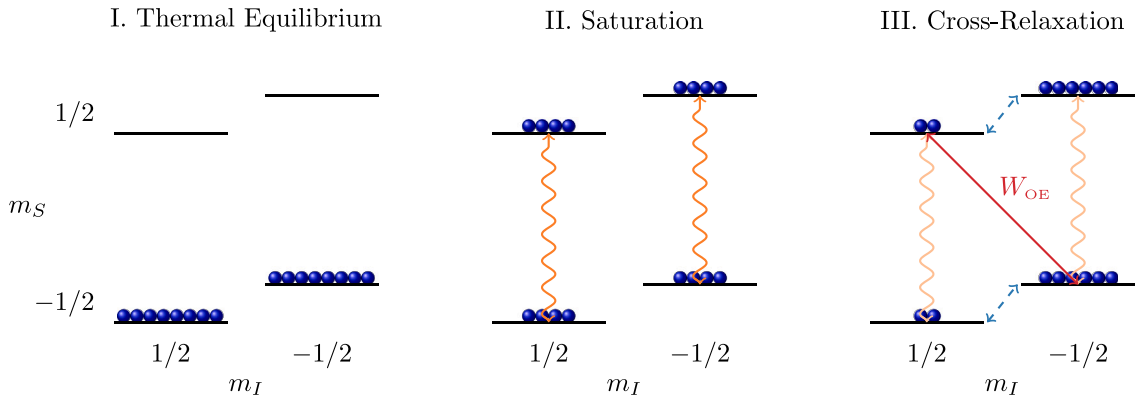

Fig. 5. Overhauser DNP. (I) In thermal equilibrium the electron spin ground state is more strongly populated than the excited states. (II) The electron transitions are saturated using microwave irradiation. (III) A cross-relaxation mechanism W_{OE} drives the populations of the connected states towards thermal equilibrium, depleting the state $|m_S m_I\rangle = |\frac{1}{2}\,\frac{1}{2}\rangle$. The result is a strong polarization across the nuclear spin transitions (dashed blue arrows).

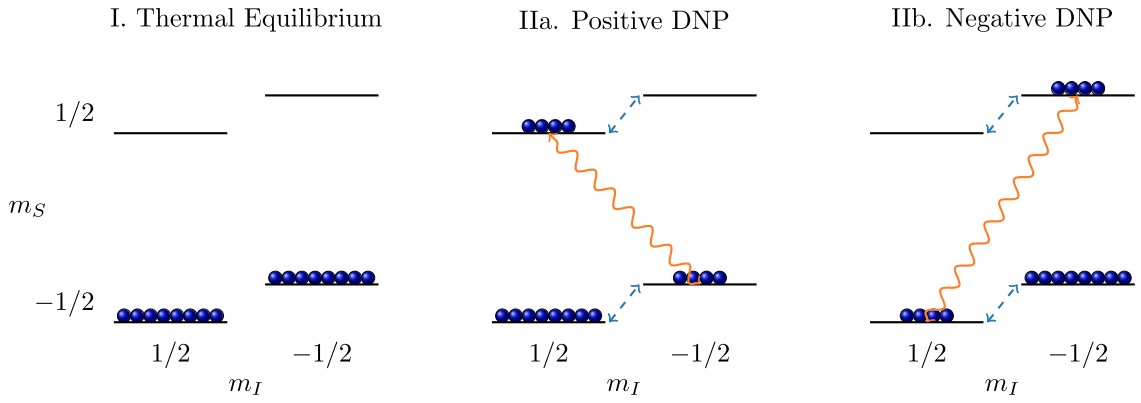

Fig. 6. The solid effect. (I) In thermal equilibrium the electron spin ground state is more strongly populated than the excited states. (IIa) Microwave irradiation at a frequency $\omega = \omega_{0s} - \omega_{0I}$ saturates the transition $|-\frac{1}{2}\,-\frac{1}{2}\rangle \leftrightarrow |\frac{1}{2}\,\frac{1}{2}\rangle$. As a result, large population imbalances are generated across the nuclear spin transitions (dashed blue arrows). These correspond to a positive NMR signal enhancement. (IIb) Microwave irradiation at a larger frequency $\omega = \omega_{0s} + \omega_{0I}$ saturates the transition $|-\frac{1}{2}\,\frac{1}{2}\rangle \leftrightarrow |\frac{1}{2}\,-\frac{1}{2}\rangle$. As a result, large population imbalances are generated across the nuclear spin transitions (dashed blue arrows). These correspond to a negative NMR signal enhancement.

effect DNP spectrum is obtained [31]. However, when this experiment is repeated at twice the field (6.7 T), the frequency separation of the peaks in the DNP spectrum does *not* double [58]. This is because the forbidden transitions in essence become more forbidden at higher fields (the product states approximate the eigenstates of the Hamiltonian (8) even better due to the increasing strength of the Zeeman interaction). Then, the microwave power that is available from solid state microwave sources used in D-DNP is no longer sufficient to drive a solid effect.

3.2.3. *Triple spin flips*

Most D-DNP experiments rely on triple spin flips, in which an electron–electron flip-flop is accompanied by a simultaneous nuclear spin flip. This mechanism is shown in Fig. 7, with the development of nuclear spin hyperpolarization unfolding as follows. First, the electrons are polarized thermally, i.e., by keeping them in a high magnetic field at low temperature. In a fully polarized sample, no electron–electron flip-flops can occur. But now, the microwave irradiation is used to flip single electron spins, and this process is followed by a triple flip comprising an electron–electron flip-flop and a nuclear spin flip. In this triple spin flip the energy change of the electron spins due to the electron–electron flip-flop is balanced by the change in nuclear Zeeman energy due to the nuclear flip.

The triple-spin-flip system comprises all of the interactions of the solid effect, but adds a second electron spin that is coupled to the first electron spin.

$$\mathcal{H}_0 = -\omega_{0I}\hat{I}_z + \omega_{0S_1}\hat{S}_{1z} + \hat{\boldsymbol{S}}_1\boldsymbol{A}\hat{\boldsymbol{I}} + \hat{\boldsymbol{S}}_1\boldsymbol{D}\hat{\boldsymbol{S}}_2 + \omega_{0S_2}\hat{S}_{2z}. \tag{10}$$

Following Wenckebach [95], if the change of the electron spin energy is due to different electron Zeeman interactions, i.e., due to g-anisotropy, the process is termed a “cross effect”. If the change of the electron spin energy is due to spin–spin interactions, the process is termed thermal mixing. Typically, both anisotropy and spin–spin interactions are at play simultaneously, and so the cross effect and thermal mixing are limiting cases of the same phenomenon, namely triple spin flips in a coupled electron–electron–nuclear spin system with g-anisotropy.

Suppose the low-frequency part of the EPR spectrum is saturated. If now the electron spin is also coupled to an electron spin in the high-frequency part of the EPR spectrum, a flip-flop of these two electrons would increase the overall energy of the two spins. If the EPR spectrum is wide compared to the nuclear Larmor frequency, then the difference in energy may match the Zeeman splitting of the nuclear spin. Then the nuclear spin can be flipped into the ground state, giving rise to a positive enhancement. Note that in samples where the electron spins are not fully polarized, the triple spin flips will occur even without microwave irradiation. If the EPR line is wide compared to the Zeeman splitting of different nuclei, then such triple spin flips will tend to equilibrate the spin temperatures of these nuclei. This is typically the case for nitroxide radicals, but the same effect is observable for narrow

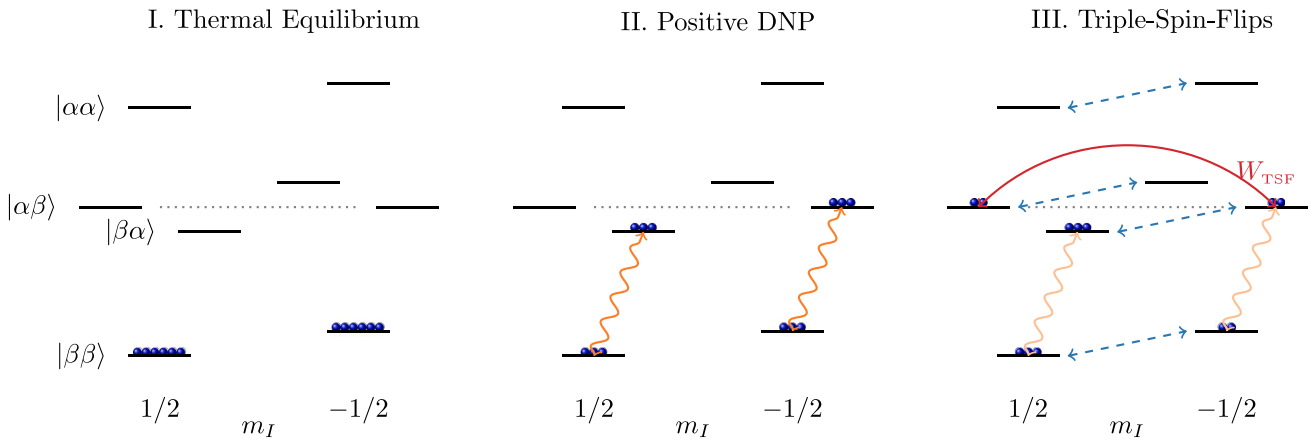

Fig. 7. Triple Spin Flips. (I) In thermal equilibrium the electron spin ground state is more strongly populated than the excited states. Note that each state is characterized by two quantum numbers for the two electron spins (such as $|\alpha\beta\rangle$), and the nuclear quantum number m_I. The product states are written as $|\alpha\beta\rangle\otimes|m_i\rangle = |\alpha\beta m_I\rangle$. Note furthermore, that the energy difference of an electron–electron flip-flop, i.e. $|\alpha\beta\rangle \leftrightarrow |\beta\alpha\rangle$ corresponds exactly to the energy difference of a nuclear spin flip, as indicated by the dotted line. This is the matching condition for triple spin flips. The energy difference between the two electron configurations can be brought about by electron Zeeman anisotropy (which is the dominant contribution in the cross effect) and/or by spin–spin interactions. (II) The two degenerate electron transitions $|\beta\beta\tfrac{1}{2}\rangle \leftrightarrow |\beta\alpha\tfrac{1}{2}\rangle$ and $|\beta\beta-\tfrac{1}{2}\rangle \leftrightarrow |\beta\alpha-\tfrac{1}{2}\rangle$ are saturated using microwave irradiation. (III) The triple spin flip $|\beta\alpha-\tfrac{1}{2}\rangle \leftrightarrow |\alpha\beta\tfrac{1}{2}\rangle$ equilibrates the populations of the participating, degenerate levels. The result is a strong positive polarization across the nuclear spin transitions (dashed blue arrows). By the same processes, applying microwave irradiation at a higher frequency (i.e. across the $|\beta\beta\rangle \leftrightarrow |\alpha\beta\rangle$ transition) would lead to negative polarization (not shown).

band trityl radicals if the nuclear Zeeman splitting is smaller than the electron–electron interactions in the sample [96–98].

Again ignoring spin diffusion, the DNP spectrum for triple spin flips may be approximated as

$$D^{\mathrm{TSF}}(\omega) \sim S(\omega)S(\omega+\omega_I) - S(\omega)S(\omega-\omega_I) \tag{11}$$

Due to the g-anisotropy of nitroxide radicals, their EPR spectra are asymmetric, with higher intensity at higher frequency. It follows that the minimum of the DNP spectrum has a larger magnitude than its maximum, i.e., a higher polarization is obtained for negative dynamic nuclear polarization.

3.3. The thermal mixing vs resonant mixing controversy

Dynamic nuclear polarization is a field that is driven heavily by experimental observations, and often these produce unexpected results. While the broadband trityl radical is not in general suited for hyperpolarizing high-γ nuclei such as protons using low-power microwave sources, Han and coworkers found that the EPR spectrum of trityl in pure DMSO broadens to approximately 300 MHz upon increasing the trityl concentration to 100 mM, and that consequently a dispersive-shaped line is obtained in the DNP spectrum [59]. Han et al. have attributed their finding to the onset of thermal mixing.

Conversely, Griffin and coworkers have shown that the EPR spectrum of trityl in DMSO-d_6:D_2O:H_2O (6:3:1) broadens only weakly when the trityl concentration is increased from 8 mM to 80 mM. They explained the dispersive-shaped line in the DNP spectra of these particular samples in terms of a mixing of states under the combined action of hyperfine interaction and microwave irradiation, a new DNP mechanism that they referred to as resonant mixing [99].

We note that these attributions do not seem to be conflicting. Both studies use the same radical, however the solvents differ, and the different solvents likely lead to the very different EPR spectra of trityl in both studies. While trityl clearly dissolves well in DMSO-d_6:D_2O:H_2O, the very broad EPR spectrum observed in DMSO indeed indicates clustering. As a side note, clustering of trityl in pyruvic acid at a low concentration of 15 mM was also invoked to account for trityl-induced ^{1}H relaxation below 100 mT, see the supporting material of Ref. [100]. This is consistent with a calculated line-broadening due to trityl clustering of up to 300 MHz [59], which precludes TM in the Griffin experiments at a ^{1}H Larmor frequency of 600 MHz, but in fact supports the notion of thermal mixing in the experiments reported by Han near a ^{1}H Larmor frequency of 300 MHz.

We refer to a recent review by Perras et al. [101] for an extended discussion of competing DNP mechanisms in mono-radicals.

3.4. Spin diffusion

The DNP mechanisms that have been discussed up to this point transfer polarization from one or two electron spins to a single nuclear spin. Spin diffusion proceeds by flip-flops of coupled spins and tends to equilibrate polarization across the network of coupled spins. In D-DNP samples, the electron spins typically form a coupled spin system, so that electron spin diffusion is active. Electron spin diffusion proceeds by electron–electron flip-flops such as $|\alpha\beta\rangle \leftrightarrow |\beta\alpha\rangle$. In favorable cases, electron spin diffusion can increase the efficiency of the DNP process. Then, the microwave may flip a remote electron, and this flipped state can diffuse to the triple spin system, where subsequently a triple spin flip may occur. This process has been called the indirect cross effect [102]. If electron spin diffusion is too efficient however, it will tend to equilibrate populations across the $|\alpha\beta\rangle \leftrightarrow |\beta\alpha\rangle$ transitions in Fig. 7, and effectively the entire EPR spectrum is saturated upon application of microwave irradiation. In this case the DNP spectra of both the solid effect and triple spin flips vanish, while the Overhauser effect is not affected.

Nuclear spin diffusion is required to distribute nuclear spin polarization across the sample. Following a discussion given by Wenckebach [103], in CaF_2, a model system for magnetic resonance [104], the ^{19}F nuclear spin diffusivity in CaF_2 is anisotropic, but is found from theoretical [105,106] and later experimental estimates [107] to be of the order of $6\times10^{-16}\mathrm{m}^2/\mathrm{s}$. For a purely dipolar spin Hamiltonian, the spin diffusivity scales as $c^{1/3}\gamma^2$, where c is a measure of spin concentration. The concentration of fluorine spins in CaF_2 is 81 M. Thus we may introduce an isotropic molar spin diffusion coefficient D_0 which we may estimate as

$$D_0 \approx \frac{6\times10^{-16}\,\mathrm{m}^2/\mathrm{s}}{(81\,\mathrm{M})^{1/3}}\left(\frac{\gamma^{^1\mathrm{H}}}{\gamma^{^{19}\mathrm{F}}}\right)^2 \approx 1.3\times10^{-16}\,\frac{\mathrm{m}^2}{\mathrm{sM}^{1/3}} \tag{12}$$

For arbitrary spins with a (molar) concentration c and a gyromagnetic ratio γ_I, the spin diffusion coefficient may then be estimated as

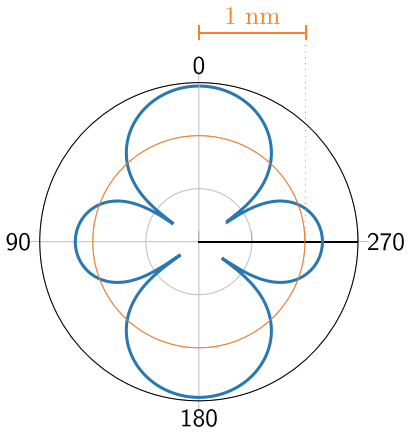

Fig. 8. The diffusion barrier is loosely defined as the surface at which the hyperfine coupling exceeds the strength of dipolar interactions. The blue line shows the surface where the electron–proton hyperfine coupling equals $2\pi\,50\,\mathrm{kHz}$.
Source: Adapted from Ref. [103].

$$D = D_0 c^{1/3} f^2 \tag{13}$$

where $f = \gamma_I/\gamma^{^1\mathrm{H}}$. The time required to spread polarization by a distance r by spin diffusion is [103]

$$t = \frac{r^2}{4D} \tag{14}$$

For $r = 1\,\mu\mathrm{m}$ and 50 M ^{1}H this expression evaluates to 7 min. For the same distance and 1 M ^{13}C labeled carbon the same expression evaluates to 7 h.

In the vicinity of the electron spin, the nuclear spins are subject to strong hyperfine couplings. Their energy levels are therefore shifted, and the flip-flops that drive nuclear spin diffusion are greatly suppressed. To describe this effect, we assume that the hyperfine interaction is weak compared to the nuclear Zeeman energy. Then, the solid effect Hamiltonian may be written as

$$\mathcal{H} = \gamma_S B\hat{S}_z - \gamma_I B\hat{I}_z + A_{zz}\hat{S}_z\hat{I}_z. \tag{15}$$

where we have assumed an isotropic electron g-tensor with $\gamma_S = \mu_B g/\hbar$.

At high-field, the eigenstates of this Hamiltonian are the product states, and the energy levels are

$$E = \gamma_S B m_S - \gamma_I B m_I + A_{zz} m_S m_I \tag{16}$$

where

$$A_{zz} = \frac{\mu_0}{4\pi}\frac{\hbar\gamma_I\gamma_S}{r_{IS}^3}\left(1 - 3\cos^2\theta\right) \tag{17}$$

is the secular part of the hyperfine interaction, with θ being the angle between the vector connecting the spins and the applied magnetic field. If A_{zz} is larger than the inter-nuclear interactions, heteronuclear flip-flops do not preserve energy, and hence their rate is reduced. For proton dipolar interactions of the order of 50 kHz, we may allow for a maximum $A_{zz} = 2\pi\,50\,\mathrm{kHz}$, and solve Eq. (17) for r. The resulting shape, shown in Fig. 8, is known as the spin diffusion barrier. It is anisotropic and vanishes at the magic angle. If we approximate the volume inside the spin diffusion barrier with a sphere of a radius of 1 nm, and assume a radical concentration of 50 mM, we find that 12% of the sample volume is located inside the diffusion barrier.

The strong hyperfine interaction exhibited by spins inside the spin diffusion barrier puts their resonance frequency out of reach of the RF pulses that are used to either detect or saturate the nuclear spins. Stern and Jannin showed that these "hidden spins" however do couple to the bulk spins [108]. In their experiment they first polarized the nuclear spins using DNP, and then switched the microwave source off and saturated the bulk spins. Afterwards they observed that the bulk nuclear spin polarization recovers to a value that is above the thermal equilibrium polarization. This spin polarization can only stem from spins inside the spin diffusion barrier that have not been affected by the saturation procedure. In a follow up study, Stern and co-workers showed that the diffusivity near an electron spin decreases substantially as the electron spin polarization increases [109]. Related effects have been observed in the context of electron decoupling in MAS DNP [110]. It should be noted that nuclear spins that are close to each other are also more likely to have a similar hyperfine coupling, and in this way one can think of the hyperfine coupling more as a "diffusion brake" than a hard barrier. As was shown recently by the group of Ernst, electron–nuclear four spin flip-flops involving one pair of electrons and one pair of nuclei may conserve energy and drive nuclear flip-flops even if the electron–nuclear hyperfine interactions differ for both nuclei [111].

In our own work, we have been able to model spin dynamics due to triple spin flips with very few parameters when the triple spin flips themselves were the rate-limiting step [100]. When the relevant interactions and relaxation parameters of a DNP process are known, it is possible to simulate the steady state of DNP experiments accurately [112]. However, many processes in D-DNP exhibit a complex, often not well-known dependence on temperature and magnetic field, and hyperpolarization strategies in D-DNP today are frequently informed largely by experiment rather than by theory. Thus, optimal sample formulations, including radical concentrations as well as the dependence of D-DNP polarization on magnetic field and temperature were all established experimentally. The situation may differ in MAS-DNP, where theoretical studies guide experimental design [14, 113].

3.5. Heteronuclear polarization transfer for D-DNP

Since spin diffusion is slow for low abundance, low-γ nuclei, it is often a good idea to polarize a more abundant spin species and then transfer this polarization to the target nucleus.

The most efficient way to transfer polarization from one spin species to another in the solid is Hartmann–Hahn cross-polarization (CP) [114], first used for ^{1}H-^{13}C cross-polarization by Pines, Gibby and Waugh [115]. The key challenge to overcome in the context of D-DNP is to generate sufficiently strong B_1 fields without causing arcing in the helium atmosphere [116,117], a challenge that becomes yet more difficult at the low vapor pressure of helium near 1 K. Under these conditions, ^{1}H-^{13}C cross-polarization has been demonstrated independently by the groups of Jannin and Ernst [118–120] and has since been extended to a range of hetero-nuclei.

An alternative approach to transfer spin polarization was first reported by Jacquinot and co-workers who polarized the abundant fluorine spins in CaF_2 (doped with Tm^{2+}) and then transferred the fluorine polarization to the low-abundance ^{43}Ca isotope using adiabatic demagnetization in the rotating frame (ADRF) [121]. More recently, this concept has been applied in the context of D-DNP to a ^{1}H - ^{13}C-transfer for ^{13}C-labeled acetate co-dissolved in a glass-forming agent with 50 mM TEMPOL by Elliot and colleagues [122].

It should be noted that one may turn both the ADRF and the CP approach around, polarize a low-γ nucleus, and transfer the resulting polarization to the abundant protons. When polarizing protons in this way, one may use narrow-band radicals, which cause smaller relaxation losses during the ensuing solid state sample transfer, which may lead to a larger liquid-state ^{1}H polarization. This approach is currently being explored in our lab.

One may also use thermal mixing to transfer polarization from one spin species to another. It is common practice to denote the spin temperature by $\beta = 1/kT$. For a reservoir of spin 1/2 nuclei, the spin temperature is obtained by solving Eq. (3) for β:

$$\beta = \frac{2\,\mathrm{arctanh}(P)}{\hbar\gamma B}. \tag{18}$$

When multiple nuclear spin species can interact with electron spins via triple spin flips, these flips will tend to equilibrate the spin temperatures of the involved species. In the high-temperature approximation, the heat capacities of the nuclear spin reservoirs scale as $\gamma^2 c$, where c is a measure of the spin concentration [123,124]. If the heat capacity of the mediating reservoir (this can be, e.g., the electron dipolar reservoir) can be neglected, then the final spin temperature of both reservoirs β_f resulting from mixing of reservoirs with initial temperatures β_1 and β_2 will be

$$\beta_f = \frac{\beta_1 \gamma_1^2 c_1 + \beta_2 \gamma_2^2 c_2}{\gamma_1^2 c_1 + \gamma_2^2 c_2} \tag{19}$$

Thus by cooling a high-abundance, high-γ reservoir to a low spin temperature and bringing it into thermal contact with a low-abundance low-γ reservoir, one may also cool the latter reservoir.

For typical concentrations, narrow-band radicals like trityl do not support triple spin flips involving protons, and thus protons do not couple to the mediating dipolar reservoir. However, when the field is lowered, the proton Zeeman interaction decreases, while electron dipolar interactions are preserved. Then, triple spin flips become possible and may be used to transfer polarization from one species to another [100]. If one reduces the applied field to values where the Zeeman interaction approaches nuclear dipolar interactions, different spin species will again tend to equilibrate their spin temperatures. This approach has been used in the context of so-called "brute-force" [3] hyperpolarization experiments. It has been found that radicals have to be removed carefully from the samples to avoid fast, radical-induced nuclear spin relaxation in the solid at low fields [4].

Polarization may also be transferred from one spin species to another in liquids by using INEPT-type sequences [125], or the Nuclear Overhauser Effect [126,127]. Very recently, a robust, J-coupling based polarization transfer at zero-field, first demonstrated in the context of PHIP experiments [128], has been shown to yield significant ^{13}C polarization also when the protons are polarized using DNP [129].

4. Sample transfer

Once the sample is polarized, it needs to be transferred and liquefied for detection near ambient temperature. We choose to categorize the existing transfer techniques into three different families. The first family is the widely established dissolution-DNP experiment (D-DNP), in which the frozen sample is hyperpolarized, and the frozen solid is then dissolved near the point of polarization using a jet of hot solvent. The second family is temperature-jump and rapid-melt DNP (TJ-DNP, RM-DNP), where hyperpolarization of the solid and liquid-state detection occur at nearby locations in the same magnet. The third family is bullet-DNP (B-DNP), where the hyperpolarized material is transferred rapidly as a solid, followed by dissolution inside the liquid-state NMR magnet near the point of detection. The key challenges that these methods address are to (i) achieve the highest possible polarization, (ii) transfer and melt the sample with minimal loss of hyperpolarization, (iii) suppress bubbles in the solution and stabilize the solution rapidly for detection, (iv) minimize sample dilution as well as radical-induced nuclear spin relaxation during acquisition and (v) perform the experiment at the highest possible rate.

4.1. Original D-DNP

A schematic diagram of the original D-DNP experiment is shown in Fig. 9. The D-DNP experiment is typically carried out at a field of 3–10 T, with the highest polarization levels attained at temperatures near 1 K. The required microwave power is in the range of 10 to 100 mW, and immersion of the frozen sample in liquid helium is required to effectively cool the sample during hyperpolarization. For dissolution, the sample is lifted out of the liquid helium bath, and then washed out using a jet of superheated solvent. This landmark experiment, first described by Ardenkjær-Larsen, Golman and co-workers [31], has been translated to pre-clinical and eventually human *in vivo* studies within only 10 years [32].

For applications of original D-DNP in NMR spectroscopy, a high-pressure system for rapid injection, first described by Bowen and Hilty, enables dissolution and transfer of the hyperpolarized material within 1.2 s [130]. Using a drive pressure of 18 bar, this system uses back pressure to avoid sample degassing and to redissolve small gas bubbles. A similar Arduino™-controlled system was later presented by Katsikis, Günther and co-workers [131] and was used also in the group of Frydman [126]. The group of Jannin later described a system for fast transfer over extended distances up to 10 m [132].

It should be noted that organic solvents like methanol with their low viscosity and low surface tension are much less prone to cause line-broadening than aqueous solutions [133]. It appears that original D-DNP experiments require a solvent amount of the order of 1 mL to prevent freezing and blockages during the dissolution procedure. While it is possible to bring in additional heat by using water and an immiscible organic phase, it has been found that residues of the organic phase cause substantial line broadening, limiting the applicability of this approach [134].

For a fast transfer, it is desirable to have the polarizer and the secondary magnet as close to each other as possible. Nuclear spin relaxation can be further mitigated by magnetic tunnels that generate a field of up to 1 T along the transfer path. This strategy may effectively reduce radical-induced nuclear spin relaxation that is otherwise exacerbated at low fields [135]. Since the magnetic field in general changes its direction along the transfer trajectory, it is important that these changes occur adiabatically, i.e., more slowly than the Larmor frequency. An approach that rigorously maximizes the magnetic field along the transfer path is the "dual iso-centre" magnet in which the polarizer and the liquid-state NMR magnet are stacked on top of each other within a single dewar [136]. While such a strategy has clear benefits for sample transfer times, the engineering and maintenance challenges of closely integrating two complex instruments, with demanding design requirements, should not be taken lightly.

The duty cycle of the D-DNP experiment is governed by several characteristics. The DNP process is slow for direct ^{13}C hyperpolarization, which typically takes 2 h, and may take longer for more dilute spin systems than ^{13}C-labeled neat pyruvic acid. Consequently polarizers have been developed in which several samples can be polarized simultaneously [137,138]. Parallel polarization is also implemented in the SpinLab™, a commercial D-DNP polarizer for clinical research marketed by GE HealthCare [139]. The throughput can be accelerated by making use of ^{1}H hyperpolarization, possibly in conjunction with one of the hetero-nuclear polarization transfer schemes discussed above. Then one may be limited by the cooling power of the polarizer. Here, the SpinLab uses a protocol for sample and fluid-path insertion that carefully minimizes the heat introduced into the helium bath [139]. Early D-DNP systems typically consumed liquid helium and had ample cooling power. Over the past decade however, most new DNP systems have been cryogen-free systems, in which a coldhead is used for condensing helium. While cryogen-free systems are timely in view of the shortage and expense of helium, they have limited cooling power, which reduces the number of samples that can be inserted and dissolved over a given period of time. This may be a reason why most laboratories cannot routinely perform more than 10 hyperpolarized D-DNP experiments per day. Thus far, no fully automated loading and unloading of D-DNP experiments has been reported, so that D-DNP systems can only operate fully during working hours.

4.2. Temperature-jump and rapid-melt DNP

Rather than dissolving the hyperpolarized solid with warm solvent, one may try to melt it rapidly without additional solvent. The

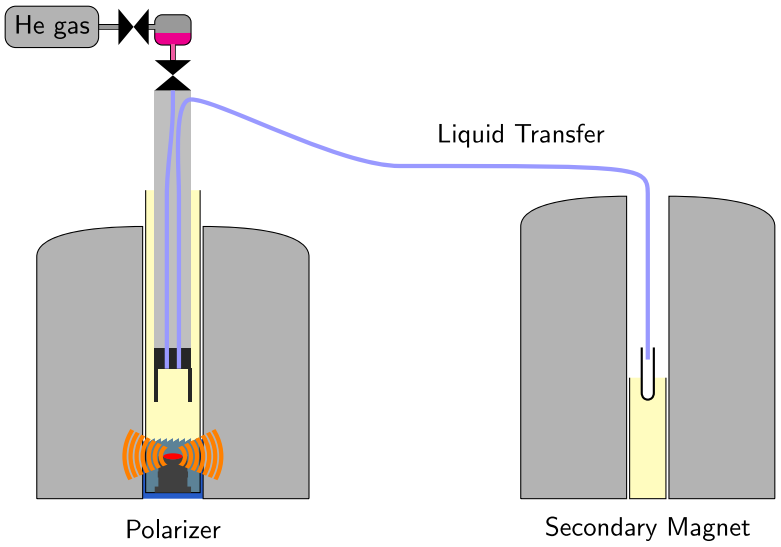

Fig. 9. Schematic diagram of the original D-DNP experiment as reported by Ardenkjær-Larsen, Golman and co-workers [31]. The sample is placed in a sample cup in a polarizer magnet (left), immersed in liquid helium, and hyperpolarized by using microwave irradiation. The sample is then lifted out of the helium bath and connected to a dissolution wand. Superheated solvent is pushed through the tubing in the dissolution wand and only the sample is dissolved. The dissolved material is subsequently transferred to a secondary magnet (right) where liquid-state NMR spectra can be recorded.

advantage of such a strategy is that the sample can afterwards be frozen again. By refreezing, repolarizing, remelting and remeasuring the same sample, multi-dimensional NMR spectra can be recorded on the same sample. The first experiment of this kind was described by the group of Griffin in 2006 and was named temperature jump DNP (TJ-DNP) [140]. They used a 10 W CO_2 laser with a wavelength of 10.6 μm to melt frozen glassy samples within 1 s, and observed ^{13}C enhancements of $\gtrsim 100$ at 5 T and 300 K. The technique was later extended to acquire 2D ^{13}C-^{13}C correlation spectra [141].

A related technique dispenses with the laser and instead uses a heated metal block to rapidly melt the sample. A rapid-melt DNP (RM-DNP) setup, as first presented in 2016 by Sharma, Kentgens and co-workers and later refined by van Meerten [142,143] is shown in Fig. 10. The sample is placed in a capillary and frozen inside the NMR magnet using liquid nitrogen, with DNP carried out at 77 K. The sample capillary is then moved into a heated copper block for rapid melting, and finally into a stripline detector [144] for liquid-state NMR detection. A key advantage of the rapid-melt DNP experiment is that it can be repeated — by lowering the capillary back into the cold zone. Due to the higher temperature of the DNP stage compared to the original D-DNP implementation, and the correspondingly shorter electron spin T_1, a klystron is required to drive the DNP process. While the attained enhancements are lower than those achieved using D-DNP, the rapid buildup of spin polarization, the possibility to signal average and the absence of dilution offer ample compensation. The linewidths attained with RM-DNP are not yet on a par with what has been achieved for D-DNP, although it is difficult to see a fundamental limitation. Furthermore it is possible to preload a capillary with several samples [145], such that these can be studied in series, possibly unattended. Efforts to combine RM-DNP with hyperpolarizing solids [146] have recently been described by the group of Jannin [147].

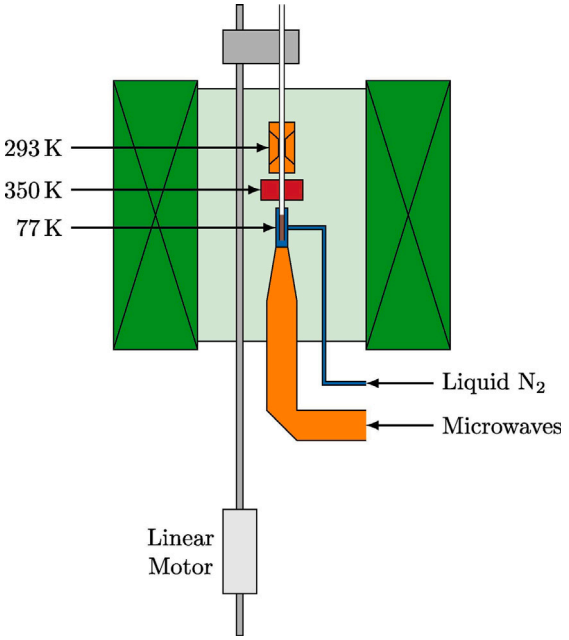

Fig. 10. In rapid-melt DNP a sample is placed in a capillary and hyperpolarized at 77 K using high-power microwave irradiation as provided by a klystron. The sample is then moved into a heated copper block, causing it to melt. For detection, the sample is moved into a stripline detector. The experiment can be repeated and multi-dimensional NMR spectra can be recorded.
Source: Figure reproduced from Ref. [142].

4.3. Bullet-DNP

In bullet-DNP, shown in Fig. 11, the hyperpolarized solid is not dissolved inside the polarizer, but transferred rapidly to the secondary magnet in solid form [148,149]. The dissolution is carried out in the secondary magnet, either directly in the NMR tube or in a solvent reservoir located above the NMR tube. A similar experiment without DNP has been reported by Kempf and co-workers under the term "brute-force hyperpolarization" [3]. In the brute-force technique, one attempts to equilibrate proton spins at very low temperature and high magnetic field. The sample is then transferred in solid form. During the transfer, low-field thermal mixing at fields below approximately 10 mT can be used to transfer polarization from ^{1}H to hetero-nuclei such as ^{13}C [4]. The transfer is carried out relatively slowly (over one second) to provide sufficient time for low-field thermal mixing. Care is taken to remove radicals such as molecular oxygen from the sample since they cause fast nuclear spin relaxation at low fields. By comparison,

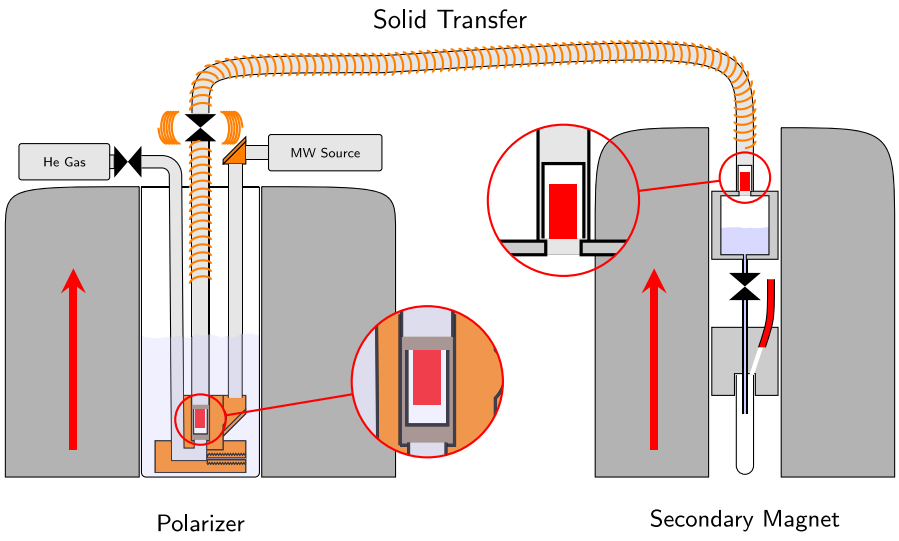

Fig. 11. The original bullet-DNP experiment as reported in Ref. [148]. The sample (red) is placed in a plastic capsule (the bullet, white), and polarized inside a polarizer (left). The lower magnified view shows the filled bullet inside the polarizer. After polarization, a magnetic tunnel is energized to a field of approximately 60 mT, and the sample is shot into a solvent reservoir located inside the secondary magnet (right). The upper magnified view shows the bullet as it arrives on top of the solvent reservoir. A restriction in the path diameter stops the bullet, and the sample is propelled into the solvent. The sample is dissolved and the resulting liquid is transferred into an NMR tube for detection.

in bullet-DNP radicals are required for hyperpolarization prior to the sample transfer, and one tries to outpace nuclear spin relaxation by transferring the sample on a timescale that is short compared to the radical-induced relaxation.

This idea was born out of our rediscovery of "tube mail": In the context of spin isomer conversion of endohedral water in the molecular endofullerene $H_2O@C_{60}$ [150,151], we wanted to measure the conversion of para-water (which, like para-hydrogen, does not give an NMR signal) back to ortho-water (which gives an NMR signal). To do so, the sample needed to be transferred rapidly from a helium-cooled environment into ambient temperature solution, with as little dilution as possible. However, the nuclear spin polarization did not need to be preserved. After several failed attempts we decided to use pressurized helium to shoot the sample from the cryostat into an NMR tube preloaded with solvent. To protect the sample during transfer, small plastic buckets were used, which were soon called "bullets". Para-to-ortho conversion was indeed observed at ambient temperature [26], and two lessons were learned from this experiment. The first lesson concerned the evolution of the spin density operator. In NMR, this evolution is typically described by the master equation

$$\dot{\rho}(t) = -i\left[\mathcal{H}_{\text{coh}}, \rho(t)\right] + \hat{\Gamma}(\rho(t) - \rho_{\text{eq}}) \tag{20}$$

where ρ is the spin density operator, $\mathcal{H}_{\text{coh}}$ is the coherent spin Hamiltonian, and $\hat{\Gamma}$ is the relaxation superoperator [152]. This equation however fails for spin systems that are far from thermal equilibrium. Instead, Bengs and Levitt used Lindblad techniques to successfully model the observed behavior [26,153]. The second lesson was of a more practical kind — the samples were traveling rather rapidly. A home-built "speedometer" that used optical detectors first employed by Katsikis [131] showed that the bullets were traveling at speeds of the order of 100 m/s (Fig. 12) .

To exploit these speeds for DNP, it is necessary to keep the spins aligned during the transfer or, in other words, apply a magnetic field such that the Zeeman interaction is much stronger than dipolar interactions. A back of the envelope calculation showed that a field of tens of mT could be obtained using commercially available DC power supplies and solenoids with a wire thickness of the order of 1 mm. The solenoids extended into both the polarizer magnet and the secondary magnet to provide a sufficiently strong magnetic field along the entire transfer path.

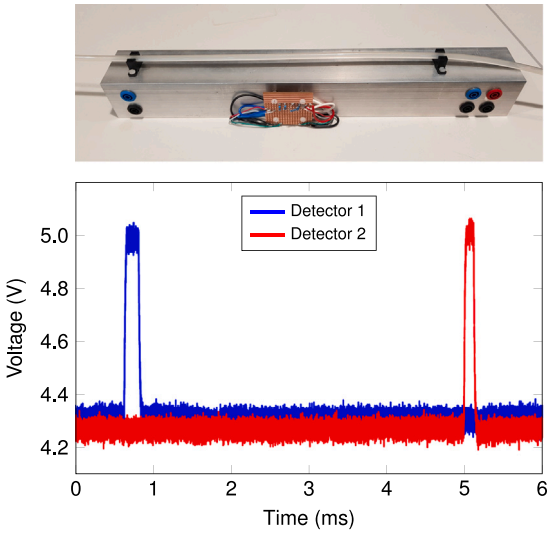

Fig. 12. (Top) The bullet speedometer. Two optical detectors, spaced 30 cm apart, measure the passage of the bullet. The photo current is measured as a voltage drop across a resistor using an oscilloscope. (Bottom) Representative data showing that the bullet needs approximately 4 ms to travel from one detector to the other (30 cm), i.e., it travels at an average velocity of approximately 75 m/s.

This tunnel design indeed preserved much of the magnetization, and led to the first demonstration of bullet-DNP by Kouřil et al. in 2019 [148], reporting a 30 % polarization in the liquid state at less than 10-fold dilution (the bullet carried a frozen solid of 80 µL which was dissolved in 700 µL of D_2O) and with a time between sample ejection from the polarizer and start of the NMR acquisition of 0.9 s. The achieved resolution however was poor, with a reported linewidth of 30 Hz.

Since then, B-DNP has been combined with important innovations that had already been implemented for conventional dissolution-DNP experiments. These include the application of back pressure to improve resolution [130] and the use of cryogen-free magnets [58,154]. While the use of cryogen-free systems is predominantly motivated by lower

operating costs, the implementation of the back-pressure technique improved the resolution of ^{13}C spectra to 2 Hz or 20 ppb [149]. In 2022, we reported field-cycling experiments that indicate tolerable relaxation during transfer for both ^{13}C [98] and ^{1}H in the presence of trityl [100]. Since then we have explored the sensitivity limits of bullet-DNP [61] and used the method to measure lifetimes of long-lived ^{1}H states [155]. Bullet-DNP was employed for the study of carbonate mineralization [156] and for storing spin polarization in carbonate matrices with a view towards MRI applications [81]. Recently, Fukazawa, Kagawa and co-workers at Osaka University used ^{31}P hyperpolarized by bullet-DNP to observe the enzymatic hydrolysis of pyrophosphates [47].

The three different implementations of the D-DNP experiment that have been discussed each offer their respective advantages. The original D-DNP experiment is the most mature technique with the widest user base, and routinely achieves high nuclear spin polarization, in particular for low-γ nuclei. The TJ-DNP and RM-DNP experiments presently achieve smaller enhancements, but are dilution-free and can be repeated for multidimensional spectroscopy. The B-DNP experiment is the youngest implementation, and offers enhancements similar to the original D-DNP experiment, but with reduced dilution.

5. Automation and the future

The power of NMR spectroscopy derives from the detailed structural and dynamic information that it can provide. However, NMR spectroscopy would be a far less accomplished methodology if the acquisition of every single spectrum required one or more highly trained scientists to operate the instrument. To the contrary, NMR instruments are often highly automated with sample changers that enable unsupervised measurements for many days. Although hyperpolarization can be achieved in tens of minutes for protons and, via cross-polarization and similar technologies, also for low-γ nuclei, so far no laboratory has managed to run the 50 or so experiments that should, in principle, be possible in 24 h, let alone sustain such a throughput over several days. It is likely that the future significance of D-DNP as a sensitivity enhancement modality for NMR spectroscopy hinges on whether protocols and instrumentation can be engineered to achieve this engineering feat.

Declaration of competing interest

The authors declare the following financial interests/personal relationships which may be considered as potential competing interests: Benno Meier reports financial support was provided by Karlsruhe Institute of Technology. Benno Meier reports a relationship with HyperSpin Scientific that includes: board membership. If there are other authors, they declare that they have no known competing financial interests or personal relationships that could have appeared to influence the work reported in this paper.

Acknowledgments

I thank Karel Kouřil for his many invaluable contributions to bullet-DNP, and Hana Kouřilová for helping to get the bullets flying. I am indebted to my entire group at KIT for their unwavering commitment. I thank Walter Köckenberger, Josef Granwehr, Malcolm Levitt and Tom Wenckebach for support throughout the “DNP years”. I thank Quentin Stern for reading the manuscript and providing many useful additions and corrections. This work was supported by the Helmholtz Associations’ Initiative and Networking (Impuls- und Vernetzungsfonds) Fund (grant VH-NG-1432) and received funding from the European Research Council (ERC) under the European Union’s Horizon 2020 Research and Innovation program (grant agreement no. 951459) and the DFG (grant number 454252029 - SFB 1527). Parts of this work have been submitted as a habilitation thesis at Karlsruhe Institute of Technology.

Glossary of abbreviations

BDPA: 1,3-bisdiphenylene-2-phenylallyl
B-DNP: Bullet-Dynamic Nuclear Polarization
DNP: Dynamic Nuclear Polarization
DNP SENS: DNP Surface Enhanced NMR Spectroscopy
DMSO: Dimethyl Sulfoxide
D-DNP: Dissolution-Dynamic Nuclear Polarization
CE: Cross Effect
EPR: Electron Paramagnetic Resonance
NMR: Nuclear Magnetic Resonance
MAS: Magic Angle Spinning
MRI: Magnetic Resonance Imaging
INEPT: Insensitive Nuclei Enhanced by Polarization Transfer
CP: Cross-Polarization
CIDNP: Chemically-induced Dynamic Nuclear Polarization
PA: Polarizing Agent
PHIP: Parahydrogen-induced Polarization
QRIP: Quantum-rotor-induced Polarization
RM-DNP: Rapid-melt Dynamic-Nuclear Polarization
SE: Solid Effect
SNR: Signal-to-Noise Ratio
TEMPO: 2,2,6,6-Tetramethylpiperidin-1-oxyl
TEMPOL: 4-Hydroxy-2,2,6,6-Tetramethylpiperidin-1-oxyl
TJ-DNP: Temperature-jump Dynamic Nuclear Polarization
TM: Thermal Mixing
UV-PA: Pyruvic acid irradiated with ultraviolet light

Data availability

Data will be made available on request.

References

[1] J. Eills, D. Budker, S. Cavagnero, E.Y. Chekmenev, S.J. Elliott, S. Jannin, A. Lesage, J. Matysik, T. Meersmann, T. Prisner, J.A. Reimer, H. Yang, I.V. Koptyug, Spin hyperpolarization in modern magnetic resonance, Chem. Rev. 123 (2023) 1417–1551.

[2] K. Kouřil, B. Meier, Hyperpolarization and sensitivity in nuclear magnetic resonance, J. Magn. Reson. Open 21 (2024) 100172.

[3] M.L. Hirsch, N. Kalechofsky, A. Belzer, M. Rosay, J.G. Kempf, Brute-force hyperpolarization for NMR and MRI, J. Am. Chem. Soc. 137 (2015) 8428–8434.

[4] D.T. Peat, M.L. Hirsch, D.G. Gadian, A.J. Horsewill, J.R. Owers-Bradley, J.G. Kempf, Low-field thermal mixing in [1-^{13}C] pyruvic acid for brute-force hyperpolarization, Phys. Chem. Chem. Phys. 18 (2016) 19173–19182.

[5] C.D. Jeffries, Polarization of nuclei by resonance saturation in paramagnetic crystals, Phys. Rev. 106 (1957) 164–165.

[6] A. Abragam, J. Combrisson, I. Solomon, Polarisation dynamique des noyaux du silicium 29 dans le silicium à 4.2 K, Comptes Rendus de L’Académie Des Sci. 247 (1958) 2337–2340.

[7] E.P. Saliba, E.L. Sesti, N. Alaniva, A.B. Barnes, Pulsed electron decoupling and strategies for time domain dynamic nuclear polarization with magic angle spinning, J. Phys. Chem. Lett. 9 (2018) 5539–5547.

[8] T.V. Can, J.J. Walish, T.M. Swager, R.G. Griffin, Time domain DNP with the NOVEL sequence, J. Chem. Phys. 143 (2015) 054201.

[9] K.O. Tan, C. Yang, R.T. Weber, G. Mathies, R.G. Griffin, Time-optimized pulsed dynamic nuclear polarization, Sci. Adv. 5 (2019) eaav6909.

[10] V.S. Redrouthu, G. Mathies, Efficient pulsed dynamic nuclear polarization with the X-inverse-X sequence, J. Am. Chem. Soc. 144 (2022) 1513–1516.

[11] T. Eichhorn, N. Niketic, B. van den Brandt, U. Filges, T. Panzner, E. Rantsiou, W. Wenckebach, P. Hautle, Proton polarization above 70 % by DNP using photo-excited triplet states, a first step towards a broadband neutron spin filter, Nucl. Instrum. Methods Phys. Res. Sect. A: Accel. Spectrometers, Detect. Assoc. Equip. 754 (2014) 10–14.

[12] T.R. Eichhorn, A.J. Parker, F. Josten, C. Müller, J. Scheuer, J.M. Steiner, M. Gierse, J. Handwerker, M. Keim, S. Lucas, M.U. Qureshi, A. Marshall, A. Salhov, Y. Quan, J. Binder, K.D. Jahnke, P. Neumann, S. Knecht, J.W. Blanchard, M.B. Plenio, F. Jelezko, L. Emsley, C.C. Vassiliou, P. Hautle, I. Schwartz, Hyperpolarized solution-state NMR spectroscopy with optically polarized crystals, J. Am. Chem. Soc. 144 (2022) 2511–2519.

[13] A.C. Pinon, J. Schlagnitweit, P. Berruyer, A.J. Rossini, M. Lelli, E. Socie, M. Tang, T. Pham, A. Lesage, S. Schantz, L. Emsley, Measuring nano- to microstructures from relayed dynamic nuclear polarization NMR, J. Phys. Chem. C 121 (2017) 15993–16005.

[14] N.A. Prisco, A.C. Pinon, L. Emsley, B.F. Chmelka, Scaling analyses for hyperpolarization transfer across a spin-diffusion barrier and into bulk solid media, Phys. Chem. Chem. Phys. 23 (2021) 1006–1020.

[15] A.J. Parker, A. Dey, M.U. Qureshi, J.M. Steiner, J.W. Blanchard, J. Scheuer, N. Tomek, S. Knecht, F. Josten, C. Müller, P. Hautle, I. Schwartz, P. Giraudeau, T.R. Eichhorn, J. Dumez, Solution-state 2D NMR spectroscopy of mixtures hyperpolarized using optically polarized crystals, Angew. Chem. Int. Ed. 62 (2023) e202312302.

[16] J. Matysik, A. Diller, E. Roy, A. Alia, The solid-state photo-CIDNP effect, Photosynth. Res. 102 (2009) 427–435.

[17] F. De Biasi, M.A. Hope, C.E. Avalos, G. Karthikeyan, G. Casano, A. Mishra, S. Badoni, G. Stevanato, D.J. Kubicki, J. Milani, J.-P. Ansermet, A.J. Rossini, M. Lelli, O. Ouari, L. Emsley, Optically enhanced solid-state ^{1}H NMR spectroscopy, J. Am. Chem. Soc. 145 (2023) 14874–14883, PMID: 37366803.

[18] F.D. Biasi, G. Karthikeyan, M. Visegrádi, M. Levien, M.A. Hope, P.J. Brown, M.R. Wasielewski, O. Ouari, L. Emsley, Light-induced ^{1}H NMR hyperpolarization in solids at 9.4 and 21.1 T, J. Am. Chem. Soc. 146 (2024) 19667–19672.

[19] C.R. Bowers, D.P. Weitekamp, Transformation of symmetrization order to nuclear-spin magnetization by chemical reaction and nuclear magnetic resonance, Phys. Rev. Lett. 57 (1986) 2645–2648.

[20] C.R. Bowers, D.P. Weitekamp, Parahydrogen and synthesis allow dramatically enhanced nuclear alignment, J. Am. Chem. Soc. 109 (1987) 5541–5542.

[21] R.W. Adams, J.A. Aguilar, K.D. Atkinson, M.J. Cowley, P.I.P. Elliott, S.B. Duckett, G.G.R. Green, I.G. Khazal, J. Lopez-Serrano, D.C. Williamson, Reversible interactions with para-hydrogen enhance NMR sensitivity by polarization transfer, Science 323 (2009) 1708–1711.

[22] M. Gierse, L. Dagys, M. Keim, S. Lucas, F. Josten, M.B. Plenio, I. Schwartz, S. Knecht, J. Eills, Hyperpolarizing small molecules using parahydrogen and solid-state spin diffusion, Angew. Chem. Int. Ed. 63 (2024) e202319341.

[23] J. Haupt, A new effect of dynamic polarization in a solid obtained by rapid change of temperature, Phys. Lett. A 38 (1972) 389–390.

[24] M. Icker, S. Berger, Unexpected multiplet patterns induced by the Haupt-effect, J. Magn. Reson. 219 (2012) 1–3.

[25] B. Meier, Quantum-rotor-induced polarization, Magn. Reson. Chem. 56 (2018) 610–618.

[26] B. Meier, K. Kouřil, C. Bengs, H. Kouřilová, T.C. Barker, S.J. Elliott, S. Alom, R.J. Whitby, M.H. Levitt, Spin-isomer conversion of water at room temperature and quantum-rotor-induced nuclear polarization in the water-endofullerene $H_2O@C_{60}$, Phys. Rev. Lett. 120 (2018) 266001.

[27] J.-N. Dumez, P. Håkansson, S. Mamone, B. Meier, G. Stevanato, J.T. Hill-Cousins, S.S. Roy, R.C.D. Brown, G. Pileio, M.H. Levitt, Theory of long-lived nuclear spin states in methyl groups and quantum-rotor induced polarisation, J. Chem. Phys. 142 (2015) 044506.

[28] J. Haupt, Experimental results on the dynamic nuclear polarisation in a solid by variation of temperature, Z. Naturforsch. 28a (1972) 98–104.

[29] V. Aladin, B. Corzilius, Methyl dynamics in amino acids modulate heteronuclear cross relaxation in the solid state under mas dnp, Solid State Nucl. Magn. Reson. 99 (2019) 27–35.

[30] J. Mao, V. Aladin, X. Jin, A.J. Leeder, L.J. Brown, R.C.D. Brown, X. He, B. Corzilius, C. Glaubitz, Exploring protein structures by dnp-enhanced methyl solid-state nmr spectroscopy, J. Am. Chem. Soc. 141 (2019) 19888–19901.

[31] J.H. Ardenkjær-Larsen, B. Fridlund, A. Gram, G. Hansson, L. Hansson, M.H. Lerche, R. Servin, M. Thaning, K. Golman, Increase in signal-to-noise ratio of >10,000 times in liquid-state NMR, Proc. Natl. Acad. Sci. 100 (2003) 10158–10163.

[32] S.J. Nelson, J. Kurhanewicz, D.B. Vigneron, P.E.Z. Larson, A.L. Harzstark, M. Ferrone, M. van Criekinge, J.W. Chang, R. Bok, I. Park, G. Reed, L. Carvajal, E.J. Small, P. Munster, V.K. Weinberg, J.H. Ardenkjær-Larsen, A.P. Chen, R.E. Hurd, L.-I. Odegardstuen, F.J. Robb, J. Tropp, J.A. Murray, Metabolic imaging of patients with prostate cancer using hyperpolarized [1-^{13}C]pyruvate, Sci. Transl. Med. 5 (2013) 198ra108.

[33] P. Dzien, A. Fages, G. Jona, K.M. Brindle, M. Schwaiger, L. Frydman, Following metabolism in living microorganisms by hyperpolarized ^{1}H NMR, J. Am. Chem. Soc. 138 (2016) 12278–12286.

[34] T.B. Rodrigues, E.M. Serrao, B.W.C. Kennedy, D.-E. Hu, M.I. Kettunen, K.M. Brindle, Magnetic resonance imaging of tumor glycolysis using hyperpolarized ^{13}C-labeled glucose, Nature Med. 20 (2013) 93–97.

[35] J. Kurhanewicz, D.B. Vigneron, J.H. Ardenkjaer-Larsen, J.A. Bankson, K. Brindle, C.H. Cunningham, F.A. Gallagher, K.R. Keshari, A. Kjaer, C. Laustsen, D.A. Mankoff, M.E. Merritt, S.J. Nelson, J.M. Pauly, P. Lee, S. Ronen, D.J. Tyler, S.S. Rajan, D.M. Spielman, L. Wald, X. Zhang, C.R. Malloy, R. Rizi, Hyperpolarized ^{13}C MRI: Path to clinical translation in oncology, Neoplasia 21 (2019) 1–16.

[36] J. Kurhanewicz, D.B. Vigneron, K. Brindle, E.Y. Chekmenev, A. Comment, C.H. Cunningham, R.J. DeBerardinis, G.G. Green, M.O. Leach, S.S. Rajan, R.R. Rizi, B.D. Ross, W.S. Warren, C.R. Malloy, Analysis of cancer metabolism by imaging hyperpolarized nuclei: Prospects for translation to clinical research, Neoplasia 13 (2011) 81–97.

[37] C.J. Daniels, M.A. McLean, R.F. Schulte, F.J. Robb, A.B. Gill, N. McGlashan, M.J. Graves, M. Schwaiger, D.J. Lomas, K.M. Brindle, F.A. Gallagher, A comparison of quantitative methods for clinical imaging with hyperpolarized ^{13}C-pyruvate, NMR Biomed. 29 (2016) 387–399.

[38] K.M. Brindle, J.L. Izquierdo-García, D.Y. Lewis, R.J. Mair, A.J. Wright, Brain tumor imaging, J. Clin. Oncol. 35 (2017) 2432–2438.

[39] G. Zhang, C. Hilty, Applications of dissolution dynamic nuclear polarization in chemistry and biochemistry, Magn. Reson. Chem. 56 (2018) 566–582.

[40] Y. Kim, C. Hilty, Applications of Dissolution-DNP for NMR Screening, Methods in Enzymology, Elsevier, 501–526.

[41] S. Jannin, J.-N. Dumez, P. Giraudeau, D. Kurzbach, Application and methodology of dissolution dynamic nuclear polarization in physical, chemical and biological contexts, J. Magn. Reson. 305 (2019) 41–50.

[42] S.J. Elliott, Q. Stern, M. Ceillier, T.E. Daraï, S.F. Cousin, O. Cala, S. Jannin, Practical dissolution dynamic nuclear polarization, Prog. Nucl. Magn. Reson. Spectrosc. 126–127 (2021) 59–100.

[43] A.C. Pinon, A. Capozzi, J.H. Ardenkjær-Larsen, Hyperpolarization via dissolution dynamic nuclear polarization: New technological and methodological advances, Magn. Reson. Mater. Phys. Biol. Med. 34 (2020) 5–23.

[44] J.H. Ardenkjaer-Larsen, Hyperpolarized MR - what's up doc? J. Magn. Reson. 306 (2019) 124–127.

[45] G. Zhang, F. Schilling, S.J. Glaser, C. Hilty, Reaction monitoring using hyperpolarized NMR with scaling of heteronuclear couplings by optimal tracking, J. Magn. Reson. 272 (2016) 123–128.

[46] J. Yeste, M. Azagra, M.A. Ortega, A. Portela, G. Matajsz, A. Herrero-Gómez, Y. Kim, R. Sriram, J. Kurhanewicz, D.B. Vigneron, I. Marco-Rius, Parallel detection of chemical reactions in a microfluidic platform using hyperpolarized nuclear magnetic resonance, Lab A Chip 23 (2023) 4950–4958.

[47] J. Fukazawa, Y. Mochizuki, S. Kanai, N. Miura, M. Negoro, A. Kagawa, Real-time monitoring of hydrolysis reactions of pyrophosphates with dissolution dynamic nuclear polarization, J. Phys. Chem. Lett. 15 (2024) 7288–7294.

[48] A.D. Gossert, W. Jahnke, NMR in drug discovery: A practical guide to identification and validation of ligands interacting with biological macromolecules, Prog. Nucl. Magn. Reson. Spectrosc. 97 (2016) 82–125.

[49] C. Hilty, D. Kurzbach, L. Frydman, Hyperpolarized water as universal sensitivity booster in biomolecular NMR, Nat. Protoc. 17 (2022) 1621–1657.

[50] F. Kurdzesau, B. van den Brandt, A. Comment, P. Hautle, S. Jannin, J.J. van der Klink, J.A. Konter, Dynamic nuclear polarization of small labelled molecules in frozen water-alcohol solutions, J. Phys. D: Appl. Phys. 41 (2008) 155506.

[51] E. Vaneeckhaute, C. Bocquelet, N. Rougier, S.A. Jegadeesan, S. Vinod-Kumar, G. Mathies, R. Melzi, J. Kempf, Q. Stern, S. Jannin, Dynamic nuclear polarization mechanisms using tempol and trityl OX063 radicals at 1 T and 77 K, J. Chem. Phys. 162 (2025) 154502.

[52] L. Lumata, Z. Kovacs, A.D. Sherry, C. Malloy, S. Hill, J. van Tol, L. Yu, L. Song, M.E. Merritt, Electron spin resonance studies of trityl OX063 at a concentration optimal for DNP, Phys. Chem. Chem. Phys. 15 (2013) 9800.

[53] V. Weis, M. Bennati, M. Rosay, J. Bryant, R. Griffin, High-field DNP and ENDOR with a novel multiple-frequency resonance structure, J. Magn. Reson. 140 (1999) 293–299.

[54] A. Capozzi, S. Patel, C.P. Gunnarsson, I. Marco-Rius, A. Comment, M. Karlsson, M.H. Lerche, O. Ouari, J.H. Ardenkjaer-Larsen, Efficient hyperpolarization of U-^{13}C-glucose using narrow-line UV-generated labile free radicals, Angew. Chem. Int. Ed. 58 (2018) 1334–1339.

[55] W.T. Wenckebach, Y. Quan, Monte carlo study of the spin-spin interactions between radicals used for dynamic nuclear polarization, J. Magn. Reson. 326 (2021) 106948.

[56] Benno Meier, Spinthon, 2024, https://github.com/bennomeier/spinthon.

[57] C. Hess, J. Herick, A. Berlin, W. Meyer, G. Reicherz, Measurement of electron spin-lattice relaxation times in radical doped butanol samples at 1k using the nedor method, Nucl. Instrum. Methods Phys. Res. Sect. A: Accel. Spectrometers, Detect. Assoc. Equip. 694 (2012) 69–77.

[58] J.H. Ardenkjær-Larsen, S. Bowen, J.R. Petersen, O. Rybalko, M.S. Vinding, M. Ullisch, N.C. Nielsen, Cryogen-free dissolution dynamic nuclear polarization polarizer operating at 3.35 T, 6.70 T, and 10.1 T, Magn. Reson. Med. 81 (2018) 2184.

[59] A. Equbal, Y. Li, T. Tabassum, S. Han, Crossover from a solid effect to thermal mixing ^{1}H dynamic nuclear polarization with trityl-OX063, J. Phys. Chem. Lett. 11 (2020) 3718–3723.

[60] P.T. Judge, E.L. Sesti, E.P. Saliba, N. Alaniva, T. Halbritter, S.T. Sigurdsson, A.B. Barnes, Sensitivity analysis of magic angle spinning dynamic nuclear polarization below 6 K, J. Magn. Reson. 305 (2019) 51–57.

[61] P. Narwal, N. Lorz, M. Minaei, S. Jannin, K. Kouřil, A. Gossert, B. Meier, Bullet-DNP enables NMR spectroscopy of pyruvate and amino acids at nanomolar to low micromolar concentrations, Anal. Chem. 96 (2024) 14734–14740.

[62] T. Dubroca, X. Wang, F. Mentink-Vigier, B. Trociewitz, M. Starck, D. Parker, M.S. Sherwin, S. Hill, J. Krzystek, Terahertz epr spectroscopy using a 36-tesla high-homogeneity series-connected hybrid magnet, J. Magn. Reson. 353 (2023) 107480.

[63] T.V. Can, M.A. Caporini, F. Mentink-Vigier, B. Corzilius, J.J. Walish, M. Rosay, W.E. Maas, M. Baldus, S. Vega, T.M. Swager, R.G. Griffin, Overhauser effects in insulating solids, J. Chem. Phys. 141 (2014) 064202.

[64] X. Ji, T. Can, F. Mentink-Vigier, A. Bornet, J. Milani, B. Vuichoud, M. Caporini, R. Griffin, S. Jannin, M. Goldman, G. Bodenhausen, Overhauser effects in non-conducting solids at 1.2 K, J. Magn. Reson. 286 (2018) 138–142.

[65] L. Lumata, S.J. Ratnakar, A. Jindal, M. Merritt, A. Comment, C. Malloy, A.D. Sherry, Z. Kovacs, BDPA: An efficient polarizing agent for fast dissolution dynamic nuclear polarization NMR spectroscopy, Chem. Eur. J. 17 (2011) 10825–10827.

[66] T. Cheng, A. Capozzi, Y. Takado, R. Balzan, A. Comment, Over 35 % liquid-state ^{13}C polarization obtained via dissolution dynamic nuclear polarization at 7 T and 1 K using ubiquitous nitroxyl radicals, Phys. Chem. Chem. Phys. 15 (2013) 20819.

[67] P. Miéville, P. Ahuja, R. Sarkar, S. Jannin, P.R. Vasos, S. Gerber-Lemaire, M. Mishkovsky, A. Comment, R. Gruetter, O. Ouari, P. Tordo, G. Bodenhausen, Scavenging free radicals to preserve enhancement and extend relaxation times in nmr using dynamic nuclear polarization, Angew. Chem. Int. Ed. 49 (2010) 6182–6185.

[68] V. Římal, E.I. Bunyatova, H. Štěpánková, Efficient scavenging of tempol radical by ascorbic acid in solution and related prolongation of ^{13}C and ^{1}H nuclear spin relaxation times of the solute, Molecules 29 (2024) 738.

[69] D. Gajan, A. Bornet, B. Vuichoud, J. Milani, R. Melzi, H.A. van Kalkeren, L. Veyre, C. Thieuleux, M.P. Conley, W.R. Gruning, M. Schwarzwalder, A. Lesage, C. Coperet, G. Bodenhausen, L. Emsley, S. Jannin, Hybrid polarizing solids for pure hyperpolarized liquids through dissolution dynamic nuclear polarization, Proc. Natl. Acad. Sci. 111 (2014) 14693–14697.

[70] E.V. Pokochueva, N.H. Le, S. Guibert, C. Gioiosa, Q. Stern, J. Tolchard, C. Bocquelet, O. Cala, M. Cavaillès, L. Veyre, O. Mankinen, V. Telkki, C. Thieuleux, S. Jannin, Hybrid polarizing solids with extended pore diameters for dissolution dynamic nuclear polarization, Chemistry-Methods 5 (2025) e202400068.

[71] T. Cheng, M. Mishkovsky, M.J.N. Junk, K. Münnemann, A. Comment, Producing radical-free hyperpolarized perfusion agents for in vivo magnetic resonance using spin-labeled thermoresponsive hydrogel, Macromol. Rapid Commun. 37 (2016) 1074–1078.

[72] B.C. Dollmann, M.J.N. Junk, M. Drechsler, H.W. Spiess, D. Hinderberger, K. Münnemann, Thermoresponsive, spin-labeled hydrogels as separable DNP polarizing agents, Phys. Chem. Chem. Phys. 12 (2010) 5879.

[73] T.E. Daraï, S.F. Cousin, Q. Stern, M. Ceillier, J. Kempf, D. Eshchenko, R. Melzi, M. Schnell, L. Gremillard, A. Bornet, J. Milani, B. Vuichoud, O. Cala, D. Montarnal, S. Jannin, Porous functionalized polymers enable generating and transporting hyperpolarized mixtures of metabolites, Nat. Commun. 12 (2021) 4695.

[74] T.R. Eichhorn, Y. Takado, N. Salameh, A. Capozzi, T. Cheng, J.-N. Hyacinthe, M. Mishkovsky, C. Roussel, A. Comment, Hyperpolarization without persistent radicals for in vivo real-time metabolic imaging, Proc. Natl. Acad. Sci. 110 (2013) 18064–18069.

[75] C.C. Zanella, A. Capozzi, H.A.I. Yoshihara, A. Radaelli, A.L.C. Mackowiak, L.P. Arn, R. Gruetter, J.A.M. Bastiaansen, Radical-free hyperpolarized mri using endogenously occurring pyruvate analogues and UV-induced nonpersistent radicals, NMR Biomed. 34 (2021) e4584.

[76] A. Capozzi, J.-N. Hyacinthe, T. Cheng, T.R. Eichhorn, G. Boero, C. Roussel, J.J. van der Klink, A. Comment, Photoinduced nonpersistent radicals as polarizing agents for X-nuclei dissolution dynamic nuclear polarization, J. Phys. Chem. C 119 (2015) 22632–22639.

[77] I. Marco-Rius, T. Cheng, A.P. Gaunt, S. Patel, F. Kreis, A. Capozzi, A.J. Wright, K.M. Brindle, O. Ouari, A. Comment, Photogenerated radical in phenylglyoxylic acid for in vivo hyperpolarized ^{13}C MR with photosensitive metabolic substrates, J. Am. Chem. Soc. 140 (2018) 14455–14463.

[78] M. Negroni, E. Turhan, T. Kress, M. Ceillier, S. Jannin, D. Kurzbach, Frémy's salt as a low-persistence hyperpolarization agent: Efficient dynamic nuclear polarization plus rapid radical scavenging, J. Am. Chem. Soc. 144 (2022) 20680–20686.

[79] I. Katz, A. Feintuch, R. Carmieli, S. Markovic, K. Singh, T. Harris, L. Frydman, A. Blank, Dynamic nuclear polarization enhancement of ^{13}C in glucose using electrical discharge induced radicals as polarizing agents, J. Magn. Reson. Open 10–11 (2022) 100043.

[80] A. Giannoulis, K. Butbul, R. Carmieli, J. Kim, E.T. Montrazi, K. Singh, L. Frydman, Cryogenic and dissolution DNP NMR on γ-irradiated organic molecules, J. Am. Chem. Soc. 146 (2024) 20758–20769.

[81] I. Katz, A. Schmidt, I. Ben-Shir, M. Javitt, K. Kouřil, A. Capozzi, B. Meier, A. Lang, B. Pokroy, A. Blank, Long-lived enhanced magnetization-a practical metabolic MRI contrast material, Sci. Adv. 10 (2024) eado2483.

[82] L.A. Pardi, J. Krzystek, J. Telser, L.-C. Brunel, Multifrequency EPR spectra of molecular oxygen in solid air, J. Magn. Reson. 146 (2000) 375–378.

[83] C.M. Kropf, B.V. Fine, Nonsecular resonances for the coupling between nuclear spins in solids, Phys. Rev. B 86 (2012) 094401.

[84] M. Jurkutat, K. Safiullin, P. Singh, S.L. Grage, J. Haase, B.V. Fine, B. Meier, Nuclear magnetic resonance far off the Larmor frequency: Nonsecular resonances in CaF_2, Phys. Rev. B 112 (2025) L06032.

[85] A.W. Overhauser, Polarization of nuclei in metals, Phys. Rev. 92 (1953) 411–415.

[86] T.R. Carver, C.P. Slichter, Polarization of nuclear spins in metals, Phys. Rev. 92 (1953) 212–213.

[87] C.P. Slichter, The discovery and demonstration of dynamic nuclear polarization-a personal and historical account, Phys. Chem. Chem. Phys. 12 (2010) 5741.

[88] C.P. Slichter, Principles of magnetic resonance, Springer Ser. Solid-State Sci. (1990).

[89] T.R. Carver, C.P. Slichter, Experimental verification of the Overhauser nuclear polarization effect, Phys. Rev. 102 (1956) 975–980.

[90] G. Liu, M. Levien, N. Karschin, G. Parigi, C. Luchinat, M. Bennati, One-thousand-fold enhancement of high field liquid nuclear magnetic resonance signals at room temperature, Nat. Chem. 9 (2017) 676–680.

[91] M. Bennati, T. Orlando, Overhauser DNP in Liquids on ^{13}C Nuclei, John Wiley & Sons, pp. 11–18.

[92] T. Can, Q. Ni, R. Griffin, Mechanisms of dynamic nuclear polarization in insulating solids, J. Magn. Reson. 253 (2015) 23–35.

[93] E. Erb, J.-L. Motchane, J. Uebersfled, Effet de polarisation nucléaire dans des liquids et les gaz adsorbés sur les charbons, Comptes Rendus de L'Académie Des Sci. 246 (1958) 2121–2123.

[94] K.O. Tan, M. Mardini, C. Yang, J.H. Ardenkjær-Larsen, R.G. Griffin, Three-spin solid effect and the spin diffusion barrier in amorphous solids, Sci. Adv. 5 (2019) eaax2743.

[95] W. Wenckebach, Dynamic nuclear polarization via the cross effect and thermal mixing: A. the role of triple spin flips, J. Magn. Reson. 299 (2019) 124–134.

[96] F. Jähnig, A. Himmler, G. Kwiatkowski, A. Däpp, A. Hunkeler, S. Kozerke, M. Ernst, A spin-thermodynamic approach to characterize spin dynamics in TEMPO-based samples for dissolution DNP at 7 T field, J. Magn. Reson. 303 (2019) 91–104.

[97] S.F.J. Cox, V. Bouffard, M. Goldman, The coupling of two nuclear zeeman reservoirs by the electronic spin-spin reservoir, J. Phys. C: Solid State Phys. 6 (1973) L100–L103.

[98] H. Kouřilová, M. Jurkutat, D. Peat, K. Kouřil, A.S. Khan, A.J. Horsewill, J.F. MacDonald, J. Owers-Bradley, B. Meier, Radical-induced hetero-nuclear mixing and low-field ^{13}C relaxation in solid pyruvic acid, Phys. Chem. Chem. Phys. 24 (2022) 28242–28249.

[99] Y. Quan, Y. Ouyang, M. Mardini, R.S. Palani, D. Banks, J. Kempf, W.T. Wenckebach, R.G. Griffin, Resonant mixing dynamic nuclear polarization, J. Phys. Chem. Lett. 14 (2023) 7007–7013.

[100] M. Jurkutat, H. Kouřilová, D. Peat, K. Kouřil, A.S. Khan, A.J. Horsewill, J.F. MacDonald, J. Owers-Bradley, B. Meier, Radical-induced low-field ^{1}H relaxation in solid pyruvic acid doped with trityl-OX063, J. Phys. Chem. Lett. 13 (2022) 10370–10376.

[101] F.A. Perras, F. Mentink-Vigier, S. Pylaeva, Perspectives on the dynamic nuclear polarization mechanisms of monoradicals: Overhauser effect or thermal mixing? J. Phys. Chem. Lett. 16 (2025) 3420–3432.

[102] D. Shimon, I. Kaminker, A transition from solid effect to indirect cross effect with broadband microwave irradiation, Phys. Chem. Chem. Phys. 24 (2022) 7311–7322.

[103] W. Wenckebach, Essentials of Dynamic Nuclear Polarization, Spindrift Publications, 2016.

[104] J.H.V. Vleck, The dipolar broadening of magnetic resonance lines in crystals, Phys. Rev. 74 (1948) 1168–1183.

[105] I.J. Lowe, S. Gade, Density-matrix derivation of the spin-diffusion equation, Phys. Rev. 166 (1968) 934.

[106] I.J. Lowe, S. Gade, Density-matrix derivation of the spin-diffusion equation, Phys. Rev. 156 (1967) 817–825.

[107] W. Zhang, D.G. Cory, First direct measurement of the spin diffusion rate in a homogenous solid, Phys. Rev. Lett. 80 (1998) 1324–1327.

[108] Q. Stern, S.F. Cousin, F. Mentink-Vigier, A.C. Pinon, S.J. Elliott, O. Cala, S. Jannin, Direct observation of hyperpolarization breaking through the spin diffusion barrier, Sci. Adv. 7 (2021) eabf5735.

[109] A. Chessari, S.F. Cousin, S. Jannin, Q. Stern, Role of electron polarization in nuclear spin diffusion, Phys. Rev. B 107 (2023) 224429.

[110] E.P. Saliba, E.L. Sesti, F.J. Scott, B.J. Albert, E.J. Choi, N. Alaniva, C. Gao, A.B. Barnes, Electron decoupling with dynamic nuclear polarization in rotating solids, J. Am. Chem. Soc. 139 (2017) 6310–6313.

[111] G. von Witte, S. Kozerke, M. Ernst, Two-electron two-nucleus effective hamiltonian and the spin diffusion barrier, Sci. Adv. 11 (2025) nil.

[112] S.A. Jegadeesan, Y. Zhao, G.M. Smith, I. Kuprov, G. Mathies, Simulation of pulsed dynamic nuclear polarization in the steady state, J. Chem. Phys. 163 (2025) 034111.

[113] F.A. Perras, S.L. Carnahan, W.-S. Lo, C.J. Ward, J. Yu, W. Huang, A.J. Rossini, Hybrid quantum-classical simulations of magic angle spinning dynamic nuclear polarization in very large spin systems, J. Chem. Phys. 156 (2022) 124112.

[114] S.R. Hartmann, E.L. Hahn, Nuclear double resonance in the rotating frame, Phys. Rev. 128 (1962) 2042–2053.
[115] A. Pines, M. Gibby, J. Waugh, Proton-enhanced nuclear induction spectroscopy 13c chemical shielding anisotropy in some organic solids, Chem. Phys. Lett. 15 (1972) 373–376.
[116] M. Linder, A. Hanckener, R. Ernst, Proton-enhanced carbon-13 resonance in helium-cooled probe; chemical shielding tensor of benzene, J. Magn. Reson. (1969) 35 (1979) 379–386.
[117] M.S. Conradi, Low-temperature NMR techniques, Concepts Magn. Reson. 5 (1993) 243–262.
[118] S. Jannin, A. Bornet, S. Colombo, G. Bodenhausen, Low-temperature cross polarization in view of enhancing dissolution dynamic nuclear polarization in NMR, Chem. Phys. Lett. 517 (2011) 234–236.
[119] A. Bornet, R. Melzi, A.J.P. Linde, P. Hautle, B. van den Brandt, S. Jannin, G. Bodenhausen, Boosting dissolution dynamic nuclear polarization by cross polarization, J. Phys. Chem. Lett. 4 (2013) 111–114.
[120] M. Batel, M. Krajewski, A. Däpp, A. Hunkeler, B.H. Meier, S. Kozerke, M. Ernst, Dissolution dynamic nuclear polarization efficiency enhanced by Hartmann-Hahn cross polarization, Chem. Phys. Lett. 554 (2012) 72–76.
[121] J.F. Jacquinot, W.T. Wenckebach, M. Goldman, A. Abragam, Polarization and NMR observation of ^{43}Ca nuclei in CaF_2, Phys. Rev. Lett. 32 (1974) 1096–1097.
[122] S.J. Elliott, S.F. Cousin, Q. Chappuis, O. Cala, M. Ceillier, A. Bornet, S. Jannin, Dipolar order mediated $^{1}H \rightarrow {}^{13}C$ cross-polarization for dissolution-dynamic nuclear polarization, Magn. Reson. 1 (2020) 89–96.
[123] M. Goldman, Spin Temperature and Nuclear Magnetic Resonance in Solids, Oxford University Press, 1970.
[124] A. Abragam, M. Goldman, Nuclear magnetism: Order and disorder, Int. Ser. Monogr. Phys. (1982).
[125] J. Wang, F. Kreis, A.J. Wright, R.L. Hesketh, M.H. Levitt, K.M. Brindle, Dynamic ^{1}H imaging of hyperpolarized [1-^{13}C]lactate in vivo using a reverse INEPT experiment, Magn. Reson. Med. 79 (2017) 741–747.
[126] O. Szekely, G.L. Olsen, I.C. Felli, L. Frydman, High-resolution 2D NMR of disordered proteins enhanced by hyperpolarized water, Anal. Chem. 90 (2018) 6169–6177.
[127] G. Olsen, E. Markhasin, O. Szekely, C. Bretschneider, L. Frydman, Optimizing water hyperpolarization and dissolution for sensitivity-enhanced 2D biomolecular NMR, J. Magn. Reson. 264 (2016) 49–58.
[128] F. Reineri, T. Boi, S. Aime, Parahydrogen induced polarization of ^{13}C carboxylate resonance in acetate and pyruvate, Nat. Commun. 6 (2015) 5858.
[129] Q. Stern, Q. Reynard-Feytis, S.J. Elliott, M. Ceillier, O. Cala, K. Ivanov, S. Jannin, Rapid and simple ^{13}C-hyperpolarization by ^{1}H dissolution dynamic nuclear polarization followed by an inline magnetic field inversion, J. Am. Chem. Soc. 145 (2023) 27576–27586.
[130] S. Bowen, C. Hilty, Rapid sample injection for hyperpolarized NMR spectroscopy, Phys. Chem. Chem. Phys. 12 (2010) 5766.
[131] S. Katsikis, I. Marin-Montesinos, M. Pons, C. Ludwig, U.L. Günther, Improved stability and spectral quality in ex situ dissolution DNP using an improved transfer device, Appl. Magn. Reson. 46 (2015) 723–729.
[132] M. Ceillier, Olivier angd El Daraï T. Cala, S.F. Cousin, Q. Stern, S. Guibert, S.J. Elliott, A. Bornet, B. Vuichoud, J. Milani, C. Pages, D. Eshchenko, J.G. Kempf, C. Jose, S.A. Lambert, S. Jannin, An automated system for fast transfer and injection of hyperpolarized solutions, J. Magn. Reson. Open 8–9 (2021) 100017.
[133] A. Dey, B. Charrier, K. Lemaitre, V. Ribay, D. Eshchenko, M. Schnell, R. Melzi, Q. Stern, S.F. Cousin, J.G. Kempf, S. Jannin, J.-N. Dumez, P. Giraudeau, Fine optimization of a dissolution dynamic nuclear polarization experimental setting for ^{13}C NMR of metabolic samples, Magn. Reson. 3 (2022) 183–202.
[134] T. Harris, C. Bretschneider, L. Frydman, Dissolution DNP NMR with solvent mixtures: Substrate concentration and radical extraction, J. Magn. Reson. 211 (2011) 96–100.
[135] J. Milani, B. Vuichoud, A. Bornet, P. Miéville, R. Mottier, S. Jannin, G. Bodenhausen, A magnetic tunnel to shelter hyperpolarized fluids, Rev. Sci. Instrum. 86 (2015) 024101.
[136] J. Leggett, R. Hunter, J. Granwehr, R. Panek, A.J. Perez-Linde, A.J. Horsewill, J. McMaster, G. Smith, W. Köckenberger, A dedicated spectrometer for dissolution DNP NMR spectroscopy, Phys. Chem. Chem. Phys. 12 (2010) 5883.
[137] M. Batel, M. Krajewski, K. Weiss, O. With, A. Däpp, A. Hunkeler, M. Gimersky, K.P. Pruessmann, P. Boesiger, B.H. Meier, S. Kozerke, M. Ernst, A multi-sample 94 GHz dissolution dynamic-nuclear-polarization system, J. Magn. Reson. 214 (2012) 166–174.
[138] T. Cheng, A.P. Gaunt, I. Marco-Rius, M. Gehrung, A.P. Chen, J.J. Klink, A. Comment, A multisample 7 T dynamic nuclear polarization polarizer for preclinical hyperpolarized MR, NMR Biomed. nil (2020) nil.
[139] J.H. Ardenkjær-Larsen, Introduction to dissolution DNP: Overview, instrumentation, and human applications, Handb. High Field Dyn. Nucl. Polariz. 7 (2018) 63–78.
[140] C.-G. Joo, K.-N. Hu, J.A. Bryant, R.G. Griffin, In situ temperature jump high-frequency dynamic nuclear polarization experiments: Enhanced sensitivity in liquid-state nmr spectroscopy, J. Am. Chem. Soc. 128 (2006) 9428–9432.
[141] C.-G. Joo, A. Casey, C.J. Turner, R.G. Griffin, In situ temperature-jump dynamic nuclear polarization: Enhanced sensitivity in two dimensional ^{13}C-^{13}C correlation spectroscopy in solution, J. Am. Chem. Soc. 131 (2008) 12–13.
[142] S. van Meerten, G. Janssen, A. Kentgens, Rapid-melt DNP for multidimensional and heteronuclear high-field NMR experiments, J. Magn. Reson. 310 (2020) 106656.
[143] M. Sharma, G. Janssen, J. Leggett, A. Kentgens, P. van Bentum, Rapid-melt dynamic nuclear polarization, J. Magn. Reson. 258 (2015) 40–48.
[144] P. van Bentum, J. Janssen, A. Kentgens, J. Bart, J. Gardeniers, Stripline probes for nuclear magnetic resonance, J. Magn. Reson. 189 (2007) 104–113.
[145] O. Nassar, M. Jouda, M. Rapp, D. Mager, J.G. Korvink, N. MacKinnon, Integrated impedance sensing of liquid sample plug flow enables automated high throughput NMR spectroscopy, Microsyst. & Nanoeng. 7 (2021).
[146] M. Cavaillès, A. Bornet, X. Jaurand, B. Vuichoud, D. Baudouin, M. Baudin, L. Veyre, G. Bodenhausen, J.-N. Dumez, S. Jannin, C. Copéret, C. Thieuleux, Tailored microstructured hyperpolarizing matrices for optimal magnetic resonance imaging, Angew. Chem. Int. Ed. 57 (2018) 7453–7457.
[147] C. Bocquelet, N. Rougier, H.-N. Le, L. Veyre, C. Thieuleux, R. Melzi, A. Purea, D. Banks, J.G. Kempf, Q. Stern, E. Vaneeckhaute, S. Jannin, Boosting ^{1}H and ^{13}C NMR signals by orders of magnitude on a bench, Sci. Adv. 10 (2024) eadq3780.
[148] K. Kouřil, H. Kouřilová, S. Bartram, M.H. Levitt, B. Meier, Scalable dissolution-dynamic nuclear polarization with rapid transfer of a polarized solid, Nat. Commun. 10 (2019) 1733.
[149] K. Kouřil, M. Gramberg, M. Jurkutat, H. Kouřilová, B. Meier, A cryogen-free, semi-automated apparatus for bullet-dynamic nuclear polarization with improved resolution, Magn. Reson. 2 (2021) 815–825.
[150] C. Beduz, M. Carravetta, J.Y.-C. Chen, M. Concistrè, M. Denning, M. Frunzi, A.J. Horsewill, O.G. Johannessen, R. Lawler, X. Lei, et al., Quantum rotation of ortho and para-water encapsulated in a fullerene cage, Proc. Natl. Acad. Sci. 109 (2012) 12894–12898.
[151] B. Meier, S. Mamone, M. Concistrè, J. Alonso-Valdesueiro, A. Krachmalnicoff, R.J. Whitby, M.H. Levitt, Electrical detection of ortho-para conversion in fullerene-encapsulated water, Nat. Commun. 6 (2015) 8112.
[152] R.R. Ernst, G. Bodenhausen, A. Wokaun, Principles of Nuclear Magnetic Resonance in One and Two Dimensions, Oxford University Press, Oxford, 1987.
[153] C. Bengs, M.H. Levitt, A master equation for spin systems far from equilibrium, J. Magn. Reson. 310 (2020) 106645.
[154] M. Baudin, B. Vuichoud, A. Bornet, G. Bodenhausen, S. Jannin, A cryogen-consumption-free system for dynamic nuclear polarization at 9.4 T, J. Magn. Reson. 294 (2018) 115–121.
[155] A. Razanahoera, A. Sonnefeld, K. Sheberstov, P. Narwal, M. Minaei, K. Kouřil, G. Bodenhausen, B. Meier, Hyperpolarization of long-lived states of protons in aliphatic chains by bullet dynamic nuclear polarization, revealed on the fly by spin-lock-induced crossing, J. Phys. Chem. Lett. 15 (2024) 9024–9029.
[156] E. Turhan, M. Minaei, P. Narwal, B. Meier, K. Kouřil, D. Kurzbach, Short-lived calcium carbonate precursors observed in situ via bullet-dynamic nuclear polarization, Commun. Chem. 7 (2024) 210.